Theory of optical second-harmonic generation from a sphere of centrosymmetric material: small-particle limit

Jerry I. Dadap*

Department of Physics, Columbia University, New York, New York 10027

Jie Shan

Department of Physics, Case Western Reserve University, Cleveland, Ohio 44106

Tony F. Heinz†

Departments of Physics and Electrical Engineering, Columbia University, New York, New York 10027

Received September 25, 2003; revised manuscript received February 27, 2004; accepted March 12, 2004

The electromagnetic theory of optical second-harmonic generation from small spherical particles comprised of centrosymmetric material is presented. The interfacial region where the inversion symmetry is broken provides a source of the nonlinearity. This response is described by a general surface nonlinear susceptibility tensor for an isotropic interface. In addition, the appropriate weak bulk terms for an isotropic centrosymmetric medium are introduced. The linear optical response of the sphere and the surrounding region is assumed to be isotropic, but otherwise arbitrary. The analysis is carried out to leading order in the ratio of (a/λ), the particle radius to the wavelength of the incident light, and can be considered as the Rayleigh limit for second-harmonic generation from a sphere. Emission from the sphere arises from both induced electric dipole and electric quadrupole moments at the second-harmonic frequency. The former requires a nonlocal excitation mechanism in which the phase variation of the pump beam across the sphere is considered, while the latter is present for a local-excitation mechanism. The locally excited electric dipole term, analogous to the source for linear Rayleigh scattering, is absent for the nonlinear case because of the overall inversion symmetry of the problem. The second-harmonic field is found to scale as $(a/\lambda)^3$ and to be completely determined by two effective nonlinear susceptibility coefficients formed as a prescribed combination of the surface and bulk nonlinearities. Characteristic angular and polarization selection rules resulting from the mechanism of the radiation process are presented. Various experimental aspects of the problem are examined, including the expected signal strengths and methods of determining the nonlinear susceptibilities. The spectral characteristics associated with the geometry of a small sphere are also discussed, and distinctive localized plasmon resonances are identified.

OCIS codes: 190.3970, 190.4350, 290.5850, 290.5870, 240.6680, 290.4020.

1. INTRODUCTION

Mie (1908) and Debye (1909) formulated the general theory of light scattering from a sphere at the turn of the past century.[1,2] Since then, an extensive body of literature on the linear optical properties of spherical particles has been produced, describing both theoretical and experimental extensions of the original work.[3–5] The development of lasers and nonlinear optics in the 1960s[6] paved the way for nonlinear light scattering from particles. This approach constitutes a new probing technique, one often capable of providing information not readily attainable through linear light scattering. Nonlinear optical studies for small particles have, for the most part, exploited the third-order nonlinear response[7–12] associated with effects, such as the optical Kerr effect, stimulated Brillouin and Raman scattering, and third-order sum-frequency generation.

A. Second-Order Nonlinear Response

The problem that we address in this paper concerns the *second-order nonlinear response* of a small sphere comprised of a centrosymmetric medium. It may be considered as the second-harmonic (SH) analog of linear Rayleigh scattering (LRS), a phenomenon first examined in 1871.[13] Within the electric dipole approximation, even-order harmonic generation is forbidden in the bulk of a centrosymmetric medium. The inversion symmetry, however, is broken at the surface of the medium, thus making even-order processes allowed in this region. Even-order nonlinear processes, such as second-harmonic generation (SHG), consequently exhibit a high degree of surface sensitivity for centrosymmetric media.[14–18] While this property has been developed and exploited for probing planar interfaces, it is expected to apply for all interfacial geometries. Indeed, recent experiments have clearly demonstrated the sensitivity and utility of the technique to probe the characteristics of surfaces of particles.[19–23]

Despite its importance, the limiting case of SHG from a small sphere of centrosymmetric and isotropic material has received little attention until recently. In this paper, we present such a detailed analysis, expanding upon our

earlier treatment in Ref. 24. The key feature of the present treatment is a systematic leading-order expansion beyond the electric dipole limit, for which the overall centrosymmetry of the particle implies a vanishing SH response. Before describing more completely the content of this paper, we wish to review briefly the status of related experimental and theoretical work.

B. Prior Investigations

1. Experimental

The number of experimental studies of SHG from spherical particles made of centrosymmetric media is growing. The early investigations of SHG from particles were performed on silver colloids during the 1980s.[25,26] At that time, however, the surface sensitivity of the technique was not apparent because of other possible concomitant effects, such as aggregation of particles[27] or the formation of a charge-transfer complex.[28] The surface sensitivity of SHG from spheres was unambiguously demonstrated in 1996.[19] In that study, SHG was used to probe the adsorption of dye molecules on micron-sized polystyrene particles. Subsequent experiments exploited the surface sensitivity of SHG to monitor molecular adsorption on[22,23,29] and transfer between[30] particles, to observe molecular transport across the bilayer in liposomes,[21,31,32] to measure electric surface charge and potential,[33,34] and to observe the formation of a surface charge-transfer complex.[35] Other related experiments include SHG or sum-frequency generation from nanoparticles in solutions,[36–49] from embedded[50–60] and supported[61–76] particles, from a crystalline lattice of dielectric spheres,[77,78] from an optically trapped particle,[79] from large (~50-μm to millimeter-sized) water droplets,[20,80] and even from cells.[81–84] Time-dependent measurements have also been performed to examine rotational dynamics of small asymmetric particles by SHG.[85] In a recent study, the frequency dependence of SHG from 32-nm-diameter silver particles was investigated and revealed the existence of both electric dipole and electric quadrupole localized plasmon resonances.[47] This result contrasts sharply with the case of linear Rayleigh scattering, where the electric dipole resonance contribution completely dominates the response.

2. Theoretical

The problem of the second-order nonlinear optical response of spherical particles has been examined under various approximations in previous theoretical studies. Early investigations by Agarwal and Jha[86] analyzed SHG from small metallic spheres. The authors considered the nonlinear response to arise entirely from the centrosymmetric bulk of the material, which was modeled in terms of a nonlocal nonlinear polarization.[87] Researchers later generalized this theory into a hydrodynamic formalism for SHG from particles,[88] as well as for sum- and difference-frequency generation.[89] Quantum-mechanical treatments of the material response have also been undertaken in explaining size effects of SHG in nanoparticles[50,90] and enhancement in two-dimensional quantum-dot arrays.[91] Recently, calculations of SHG from small individual and arrays of spheres under the influence of an inhomogeneous field have been presented.[92–94] SHG for dilute and highly concentrated suspensions of spherical particles has also been examined.[95]

Several investigations have been based on a simplified model of the surface nonlinear response in which the nonlinear susceptibility tensor has only a single element corresponding to all directions normal to the surface, $\chi^{(2)}_{s,\perp\perp\perp}$. This situation prevails in the model of a surface nonlinearity based on induced charges, as incorporated in the investigations of metal particles by Östling *et al.*[96] and Dewitz *et al.*[97] These treatments were carried out using the full Mie theory, as required outside of the limit of spheres small compared with the optical wavelength. SH emission from a dielectric sphere with a $\chi^{(2)}_{s,\perp\perp\perp}$ response has also been examined in the Rayleigh–Gans approximation,[78] which pertains when the refractive index of the sphere is close to that of its surroundings and affords significant simplification by eliminating the complexities of linear wave propagation. This approximation has been successful in explaining the key features of experimental SH radiation patterns from micron-sized particles.[23] Very recently, the Rayleigh–Gans approximation was applied to derive the sum-frequency field from spheres having a general isotropic nonlinear optical response.[48] The problem of SHG excited by whispering-gallery modes that occur in much larger particles has also been examined.[98]

A distinct, but related line of inquiry involves the description of surface roughness and surface-enhanced optical response. SHG from a hemispheroid, for example, was considered in this context early on.[99] In contrast to a spheroid, this structure breaks the inversion symmetry and exhibits a fully dipole-allowed SH response from the surface, even in the limit of small dimensions. A similar problem of SHG from a dense interfacial suspension of metallic colloids has also been examined.[100]

C. This Work

In the current work, we extend our earlier treatment[24] to present the general electromagnetic theory of SH Rayleigh scattering (SHRS) for small spheres of centrosymmetric material. We provide here, starting in Section 2, a complete derivation of results for the SH radiation arising from the surface nonlinear response that were initially presented in Ref. 24. In the current analysis, we also allow for an arbitrary bulk nonlinear response compatible with isotropic symmetry and obtain explicit expressions for the SH field in terms of the corresponding nonlinear susceptibilities of the material. We examine, in subsections 3.A–3.C, various features of this solution, including the physical origin of the differing contributions to the SH emission, the determination of the nonlinear material response from experimental observables, and the predicted frequency dependence of the process. We also present, in subsection 3.D, a comparison of our work with existing theories.

2. MODEL AND ITS SOLUTION

A. Model

A key aspect of our treatment of SHRS is the inclusion of the most general form of the nonlinear response compat-

ible with the assumed symmetry. Starting from this perspective, we describe the nonlinear optical response of the system phenomenologically by a nonlinear source polarization $\mathbf{P}(\mathbf{r}) = \mathbf{P}^{(2\omega)}(\mathbf{r})$ appropriate for a centrosymmetric medium and its interface.[17] This response includes both a dipole-allowed surface term and a nonlocal bulk term:

$$\begin{aligned}\mathbf{P}^{(2\omega)}(\mathbf{r}) &= \mathbf{P}^{(2\omega)}_{\text{surface}} + \mathbf{P}^{(2\omega)}_{\text{bulk}} \\ &= \vec{\vec{\chi}}^{(2)}_s : \mathbf{E}^{(\omega)}(\mathbf{r})\mathbf{E}^{(\omega)}(\mathbf{r})\,\delta(r - a) \\ &\quad + \vec{\vec{\chi}}^{(2)}_b : \mathbf{E}^{(\omega)}(\mathbf{r})\nabla\mathbf{E}^{(\omega)}(\mathbf{r}), \end{aligned} \tag{1}$$

where $\vec{\vec{\chi}}^{(2)}_s$ and $\vec{\vec{\chi}}^{(2)}_b$ are the corresponding second-order surface and bulk nonlinear susceptibilities. Here, $\mathbf{P}^{(2\omega)}(\mathbf{r})$ and $\mathbf{E}^{(2\omega)}(\mathbf{r})$ denote the complex amplitudes of the oscillating real quantities. We employ the convention that $\mathbf{P}^{(2\omega)}(\mathbf{r}, t) = 2\,\text{Re}[\mathbf{P}^{(2\omega)}(\mathbf{r})\exp(-2i\omega t)]$ for the nonlinear polarization, and correspondingly for $\mathbf{E}^{(\omega)}(\mathbf{r})$ and for other oscillating quantities introduced below.

We now describe the two nonlinear sources in more detail. We make no assumptions about the nature of the interface other than that it exhibits isotropic symmetry with a mirror plane perpendicular to the interface. The nonlinear susceptibility tensor $\vec{\vec{\chi}}^{(2)}_s$ then has three nonvanishing and independent elements: $\chi^{(2)}_{s,\perp\perp\perp}$, $\chi^{(2)}_{s,\perp\parallel\parallel}$, and $\chi^{(2)}_{s,\parallel\perp\parallel} = \chi^{(2)}_{s,\parallel\parallel\perp}$, where $\perp$ and $\parallel$ refer to the local spatial components perpendicular and parallel to the surface.[101] The susceptibility $\vec{\vec{\chi}}^{(2)}_s$ can be written, in terms of the unit vectors for the spherical coordinate system, as the triadic

$$\begin{aligned}\vec{\vec{\chi}}^{(2)}_s &= \chi^{(2)}_{s,\perp\perp\perp}\hat{\mathbf{r}}\hat{\mathbf{r}}\hat{\mathbf{r}} + \chi^{(2)}_{s,\perp\parallel\parallel}\hat{\mathbf{r}}(\hat{\boldsymbol{\theta}}\hat{\boldsymbol{\theta}} + \hat{\boldsymbol{\varphi}}\hat{\boldsymbol{\varphi}}) + \chi^{(2)}_{s,\parallel\perp\parallel}(\hat{\boldsymbol{\theta}}\hat{\mathbf{r}}\hat{\boldsymbol{\theta}} \\ &\quad + \hat{\boldsymbol{\varphi}}\hat{\mathbf{r}}\hat{\boldsymbol{\varphi}} + \hat{\boldsymbol{\theta}}\hat{\boldsymbol{\theta}}\hat{\mathbf{r}} + \hat{\boldsymbol{\varphi}}\hat{\boldsymbol{\varphi}}\hat{\mathbf{r}}). \end{aligned} \tag{2}$$

The case of an isotropic interface *lacking* a mirror plane is also of considerable interest. Such symmetry is present in a chiral interface, as would result from the adsorption of chiral molecules on an isotropic surface. In this situation, an extra independent tensor element is present, namely, $\chi^{(2)}_{s,\parallel'\parallel''\perp} = \chi^{(2)}_{s,\parallel'\perp\parallel''} = -\chi^{(2)}_{s,\parallel''\parallel'\perp} = -\chi^{(2)}_{s,\parallel''\perp\parallel'}$, where $\parallel'$ and $\parallel''$ are two distinct and orthogonal spatial components parallel to the interface.[17] Following the procedures below in the relevant small-particle approximation, one can, however, show that the additional chiral nonlinear response does not contribute to the radiated fields. Thus the results of this paper also hold true for small spheres with isotropic *chiral* surfaces.

With respect to the bulk of the sphere, the nonlinear response of the centrosymmetric bulk shown to leading-order in nonlocality in Eq. (1) can be simplified for an isotropic medium. In this case, we have

$$\mathbf{P}^{(2\omega)}_{\text{bulk}}(\mathbf{r}) = \gamma\nabla(\mathbf{E}^{(\omega)}_{\text{in}} \cdot \mathbf{E}^{(\omega)}_{\text{in}}) + \delta'(\mathbf{E}^{(\omega)}_{\text{in}} \cdot \nabla)\mathbf{E}^{(\omega)}_{\text{in}}, \tag{3}$$

where the two parameters, γ and δ', define the bulk response[87] and we have written $\mathbf{E}^{(\omega)}_{\text{in}}$ to denote the driving fundamental field within the sphere. We have omitted a term proportional to $\mathbf{E}^{(\omega)}_{\text{in}}(\nabla \cdot \mathbf{E}^{(\omega)}_{\text{in}})$, since it vanishes by Maxwell's equations in the homogeneous bulk of the material.[102]

The linear optical response of the system also plays a key role in the radiation problem. We describe it in terms of three distinct regions: the ambient medium, the interior of the sphere, and the interfacial region. These regions are characterized, respectively, by the dielectric functions ε_1, ε_2, and ε'. All dielectric functions are assumed to be isotropic, but are allowed to be dispersive. In keeping with the assumption of a transparent ambient, the quantity ε_1 is taken as real and positive, while ε_2 and ε' may be complex. The corresponding magnetic permeabilities are denoted as μ_1, μ_2, and μ'. These quantities can all be set to 1 without loss of generality for optical frequencies.[103] We do so below, except where their inclusion is useful for elucidating the nature of the response.

Figure 1 illustrates the scattering geometry employed in this analysis. The pump radiation at the fundamental (angular) frequency of ω is taken as a plane wave. It impinges on a sphere of radius a comprised of isotropic and centrosymmetric material (as described above) with a wave vector of $\mathbf{k}_1 = k_1\hat{\mathbf{k}}$. The direction of propagation defines the z axis of our coordinate system ($\hat{\mathbf{z}} = \hat{\mathbf{k}}$). The wave vector of the scattered SH radiation is given by $\hat{\mathbf{K}}_1 = K_1\hat{\mathbf{K}}$, where $\hat{\mathbf{K}} = \hat{\mathbf{r}} = \sin\theta\cos\varphi\hat{\mathbf{x}} + \sin\theta\sin\varphi\hat{\mathbf{y}} + \cos\theta\hat{\mathbf{z}}$ in terms of the unit vectors of the spherical or Cartesian coordinate systems. We define an arbitrary polarization state of the pump radiation as a unit vector $\hat{\boldsymbol{\epsilon}}_0 = \xi\hat{\mathbf{x}} + \eta\hat{\mathbf{y}}$, with complex coefficients (ξ, η) satisfying $|\xi|^2 + |\eta|^2 = 1$. For linearly polarized incident light, we write the polarization state as $\hat{\boldsymbol{\epsilon}}_0 = \cos\psi\hat{\mathbf{x}} + \sin\psi\hat{\mathbf{y}}$, where ψ is the angle of the electric field vector with respect to the $\hat{\mathbf{x}}$ axis. The polarization of the scattered SH radiation may be resolved by employing an analyzer placed between the scatterer and the detector. We describe the detected polarization state by the unit vector $\hat{\boldsymbol{\epsilon}}$.

In the analysis that follows, we assume that the sphere radius a is much smaller than the wavelength λ of the pump radiation and that the detection point is in the far field. Mathematically, we can express this set of conditions as $a/\lambda \ll 1 \ll r/\lambda$, where r is the distance to the observation point.

B. Second-Harmonic Radiation

1. Derivation of Radiated Fields

For conceptual clarity, we first consider the case of a homogeneous system in which the dielectric functions are

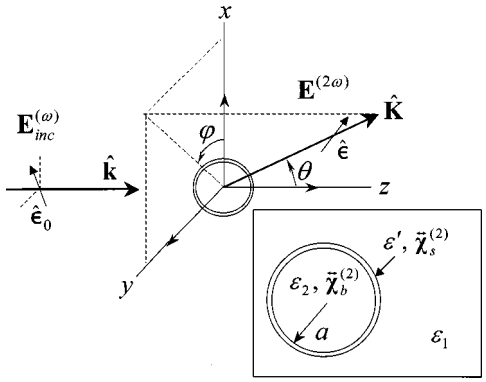

Fig. 1. Scattering geometry and the linear and nonlinear response of the small sphere for the SHRS problem. $\hat{\mathbf{k}}$ denotes the direction of the incident plane wave of polarization $\hat{\boldsymbol{\epsilon}}_0$; $\hat{\mathbf{K}}$ denotes the direction of the scattered light with polarization state $\hat{\boldsymbol{\epsilon}}$. Inset indicates the linear and nonlinear optical responses in the three regions: ambient, interface, and the internal volume of the sphere.

all identical, $\varepsilon_1 = \varepsilon_2 = \varepsilon'$, and lossless. For the general situation of three distinct dielectric constants, treated in subsection 2.B.3 below, the results for the homogeneous problem can still be applied, but with suitable corrections to account for the effect of the linear optical response at the fundamental and harmonic frequencies. Under the neglect of a dielectric discontinuity, the SH radiation problem can be solved directly by a calculation of the nonlinear source polarization and application of well-established relations for the vector potential from a given current distribution. In accordance with our interest in the response from a small particle, the nonlinear source and radiation patterns are expressed in terms of multipole moments, and only the lowest-order nonvanishing terms are retained.

Let us first briefly review some familiar electrodynamics concepts necessary for the calculations.[104] For a system with a time variation described by a frequency $\Omega = Kc$, we obtain the vector potential $\mathbf{A}(\mathbf{r})$, in the Lorentz gauge, from a current density source $\mathbf{J}(\mathbf{r}')$ as

$$\mathbf{A}(\mathbf{r}) = \frac{1}{c}\int \frac{\exp(iK_1|\mathbf{r}-\mathbf{r}'|)\mathbf{J}(\mathbf{r}')}{|\mathbf{r}-\mathbf{r}'|}\mathrm{d}\mathbf{r}', \tag{4}$$

where $K_1 = \varepsilon_1^{1/2}\Omega/c$ is the magnitude of the scattered wave vector $\mathbf{K}_1$; K is the magnitude of the vacuum wave vector; and $\mathbf{r}$ and $\mathbf{r}'$ denote the field and source points, respectively. The response in the far-field region is then given by

$$\mathbf{B}(\mathbf{r}) = \nabla \times \mathbf{A}(\mathbf{r}) = iK_1\hat{\mathbf{r}} \times \mathbf{A}(\mathbf{r}), \tag{5a}$$

$$\mathbf{E}(\mathbf{r}) = \frac{i}{\varepsilon_1 K}\nabla \times \mathbf{B}(\mathbf{r}) = \frac{1}{\sqrt{\varepsilon_1}}\mathbf{B}(\mathbf{r}) \times \hat{\mathbf{r}}, \tag{5b}$$

where $\hat{\mathbf{r}} = \mathbf{r}/r \equiv \hat{\mathbf{K}}$ denotes the scattering direction. The vector quantities $\mathbf{J}(\mathbf{r})$, $\mathbf{P}(\mathbf{r})$, $\mathbf{A}(\mathbf{r})$, $\mathbf{B}(\mathbf{r})$, and $\mathbf{E}(\mathbf{r})$ represent complex spatial amplitudes for the oscillating physical quantities according to the relation $\mathbf{F}(\mathbf{r}, t) = 2\,\mathrm{Re}[\mathbf{F}(\mathbf{r})\exp(-i\Omega t)]$, as above.

Imposing the small-particle limit of $K_1 r' \ll 1$, we can express Eq. (4) to its two leading orders in $(K_1 r')$ as[104]

$$\mathbf{A}(\mathbf{r}) = \frac{-iK\exp(iK_1 r)}{r}\left[\mathbf{p} - (\hat{\mathbf{r}} \times \mathbf{m}) - \frac{iK_1}{6}\mathbf{Q}(\hat{\mathbf{r}})\right], \tag{6}$$

where

$$\mathbf{p} = \int \mathbf{P}(\mathbf{r}')\mathrm{d}\mathbf{r}', \tag{7a}$$

$$\mathbf{m} = -\frac{iK}{2}\int \mathbf{r}' \times \mathbf{P}(\mathbf{r}')\mathrm{d}\mathbf{r}', \tag{7b}$$

$$\mathbf{Q}(\hat{\mathbf{r}}) = \int \{3[(\hat{\mathbf{r}}\cdot\mathbf{r}')\mathbf{P}(\mathbf{r}') + \hat{\mathbf{r}}\cdot\mathbf{P}(\mathbf{r}')\mathbf{r}'] - 2\mathbf{r}' \cdot \mathbf{P}(\mathbf{r}')\hat{\mathbf{r}}\}\mathrm{d}\mathbf{r}' \tag{7c}$$

are the electric dipole, magnetic dipole, and vector electric quadrupole moments, respectively.[105] The last quantity, $\mathbf{Q}(\hat{\mathbf{r}})$, which is related to the quadrupole moment tensor, Q_{ij}, through $Q_i(\hat{\mathbf{r}}) = \Sigma_j Q_{ij}\hat{\mathbf{r}}_j$, depends on the direction of observation. To obtain these relations in terms of the source polarization, we have employed the relation $\mathbf{J}(\mathbf{r}') = -i\Omega\mathbf{P}(\mathbf{r}')$, which follows from $\mathbf{J}(\mathbf{r}', t) = \partial\mathbf{P}(\mathbf{r}', t)/\partial t$.

Combining Eqs. (5)–(7), we can express the electric field as

$$\mathbf{E}^{(\Omega)} = \frac{K_1^2\exp(iK_1 r)}{\varepsilon_1(\Omega)r}(\hat{\mathbf{K}} \times \mathbf{p}_{\mathrm{eff}}) \times \hat{\mathbf{K}}, \tag{8}$$

where

$$\mathbf{p}_{\mathrm{eff}} = \mathbf{p} - (\hat{\mathbf{K}} \times \mathbf{m}) - \frac{iK_1}{6}\mathbf{Q}(\hat{\mathbf{K}}). \tag{9}$$

We now apply this formalism to describe the SHG from small spheres. To this end, we need to calculate the moments given by Eqs. (7a)–(7c) for the relevant nonlinear source polarization $\mathbf{P}(\mathbf{r}) = \mathbf{P}^{(2\omega)}(\mathbf{r})$ at the SH frequency $\Omega = 2\omega = Kc$. We treat the incident fundamental field, $\mathbf{E}_{\mathrm{inc}}^{(\omega)}(\mathbf{r})$, as a plane wave propagating along $\hat{\mathbf{k}}$ and having a general (complex) polarization state $\hat{\boldsymbol{\epsilon}}_0$:

$$\mathbf{E}_{\mathrm{inc}}^{(\omega)}(\mathbf{r}) = E_0\exp(i\mathbf{k}_1 \cdot \mathbf{r})\hat{\boldsymbol{\epsilon}}_0, \tag{10}$$

where $k_1 = |\mathbf{k}_1| = \varepsilon_1^{1/2}(\omega)k = \varepsilon_1^{1/2}(\omega)(\omega/c)$. Since the dielectric constants inside and outside the polarization shell are assumed to be equal, the plane waveform of the fundamental field is not disturbed by the presence of the sphere, i.e., $\mathbf{E}^{(\omega)}(\mathbf{r}) = \mathbf{E}_{\mathrm{inc}}^{(\omega)}(\mathbf{r}) = \mathbf{E}_{\mathrm{in}}^{(\omega)}(\mathbf{r})$. Substituting Eq. (10) into Eq. (1) and using Eqs. (2) and (3), we then obtain for the nonlinear source polarization,

$$\begin{aligned}\mathbf{P}^{(2\omega)}(\mathbf{r}) = (&\{\chi_{s,\perp\perp\perp}^{(2)}\hat{\mathbf{r}}(\hat{\mathbf{r}}\cdot\hat{\boldsymbol{\epsilon}}_0)^2 + \chi_{s,\perp\parallel\parallel}^{(2)}\hat{\mathbf{r}}[(\hat{\boldsymbol{\theta}}\cdot\hat{\boldsymbol{\epsilon}}_0)^2 + (\hat{\boldsymbol{\varphi}}\cdot\hat{\boldsymbol{\epsilon}}_0)^2] \\ &+ 2\chi_{s,\parallel\perp\parallel}^{(2)}[\hat{\boldsymbol{\theta}}(\hat{\mathbf{r}}\cdot\hat{\boldsymbol{\epsilon}}_0)(\hat{\boldsymbol{\theta}} \cdot \hat{\boldsymbol{\epsilon}}_0) + \hat{\boldsymbol{\varphi}}(\hat{\mathbf{r}}\cdot\hat{\boldsymbol{\epsilon}}_0) \\ &\times(\hat{\boldsymbol{\varphi}}\cdot\hat{\boldsymbol{\epsilon}}_0)]\}\delta(r-a) + i\gamma 2k_1\hat{\mathbf{k}}(\hat{\boldsymbol{\epsilon}}_0 \\ &\cdot \hat{\boldsymbol{\epsilon}}_0))E_0^2\exp(2i\mathbf{k}_1 \cdot \mathbf{r}).\end{aligned} \tag{11}$$

Inserting this polarization, $\mathbf{P}^{(2\omega)}$, into Eqs. (7a)–(7c), we deduce, to the lowest nonvanishing order of the product (ka) in the SH fields, the multipole moments:

$$\mathbf{p} = p_0(\hat{\boldsymbol{\epsilon}}_0 \cdot \hat{\boldsymbol{\epsilon}}_0)\hat{\mathbf{k}}, \tag{12a}$$

$$\mathbf{m} = 0, \tag{12b}$$

$$\mathbf{Q}(\hat{\mathbf{K}}) = q_0\left[(\hat{\mathbf{K}}\cdot\hat{\boldsymbol{\epsilon}}_0)\hat{\boldsymbol{\epsilon}}_0 - \frac{1}{3}(\hat{\boldsymbol{\epsilon}}_0 \cdot \hat{\boldsymbol{\epsilon}}_0)\hat{\mathbf{K}}\right]. \tag{12c}$$

Here p_0 and q_0 are complex quantities given by

$$p_0 = \frac{8\pi i}{15}k_1 a^3 E_0^2\chi_1, \tag{13a}$$

$$q_0 = \frac{16\pi}{5}a^3 E_0^2\chi_2, \tag{13b}$$

with effective nonlinear susceptibilities of

$$\chi_1 \equiv \chi^{(2)}_{s,\perp\perp\perp} + 4\chi^{(2)}_{s,\perp\parallel\parallel} - 2\chi^{(2)}_{s,\parallel\perp\parallel} + 5\gamma, \tag{14a}$$

$$\chi_2 \equiv \chi^{(2)}_{s,\perp\perp\perp} - \chi^{(2)}_{s,\perp\parallel\parallel} + 3\chi^{(2)}_{s,\parallel\perp\parallel}. \tag{14b}$$

The quantity χ_1 is thus associated with the strength of the electric dipole emission, while χ_2 corresponds to the electric quadrupole emission term. Magnetic dipole emission is absent [Eq. (12b)], a consequence of the axial symmetry of the problem. Note that the second term in the expression for $\mathbf{Q}(\hat{\mathbf{K}})$ in Eq. (12c) is directed along the direction of observation ($\hat{\mathbf{K}}$). Although it would influence the near-field response, this term does not contribute to the radiated field and, henceforth, is neglected in what follows. Substituting Eqs. (12a)–(12c) into Eq. (9), we find that the SH radiation can be presented in terms of an effective dipole moment of

$$\mathbf{p}_{\text{eff}} = p_0[(\hat{\boldsymbol{\epsilon}}_0 \cdot \hat{\boldsymbol{\epsilon}}_0)\hat{\mathbf{k}} - \kappa(\hat{\mathbf{K}} \cdot \hat{\boldsymbol{\epsilon}}_0)\hat{\boldsymbol{\epsilon}}_0]. \tag{15}$$

The parameter κ, a measure of the quadrupole contribution relative to the dipole contribution, is given by

$$\kappa = iK_1 q_0/6p_0 = K_1\chi_2/k_1\chi_1. \tag{16}$$

Combining the results of Eqs. (8) and (15), we can write the explicit expression for the SH radiation field from the small sphere as[106]

$$\mathbf{E}^{(2\omega)}(\mathbf{r}) = \frac{K^2 \exp(iK_1 r)p_0}{r}[(\hat{\boldsymbol{\epsilon}}_0 \cdot \hat{\boldsymbol{\epsilon}}_0)(\hat{\mathbf{K}} \times \hat{\mathbf{k}}) \times \hat{\mathbf{K}} - \kappa(\hat{\mathbf{K}} \cdot \hat{\boldsymbol{\epsilon}}_0)(\hat{\mathbf{K}} \times \hat{\boldsymbol{\epsilon}}_0) \times \hat{\mathbf{K}}], \tag{17}$$

with a corresponding magnetic field of $\mathbf{B}^{(2\omega)}(\mathbf{r}) = \varepsilon_1^{1/2}(2\omega)\hat{\mathbf{K}} \times \mathbf{E}^{(2\omega)}(\mathbf{r})$. Importantly, these expressions also hold true even for the general case of stratified media ($\varepsilon_1 \neq \varepsilon_2 \neq \varepsilon'$), provided the quantities χ_1 and χ_2 are replaced by the modified expressions of Eqs. (27a)–(27b), as discussed below in subsection 2.B.3.

An alternative expression for the SH field may be given using an expansion in vector spherical harmonics, $\mathbf{X}_{lm}(\theta, \varphi)$, (Appendix B):

$$\mathbf{E}^{(2\omega)}(\mathbf{r}) = \frac{K^2 \exp(iK_1 r)p_0}{r}\sum_{l=1}^{2}\sum_{\substack{m=-l \\ \text{(even)}}}^{l} c_{lm}\hat{\mathbf{r}} \times \mathbf{X}_{lm}(\theta, \varphi). \tag{18}$$

This form facilitates the identification of the different multipole modes with the $l = 1$ terms corresponding to electric dipole contributions and the $l = 2$ terms to electric quadrupole emission. The nonvanishing expansion coefficients are $c_{10} = -2i(2\pi/3)^{1/2}(\xi^2 + \eta^2)$, $c_{20} = -\kappa i(2\pi/15)^{1/2}(\xi^2 + \eta^2)$, and $c_{2,\pm 2} = \kappa i(\pi/5)^{1/2}(\xi \mp i\eta)^2$ for a general input polarization state of $\hat{\boldsymbol{\epsilon}}_0 = \xi\,\hat{\mathbf{x}} + \eta\,\hat{\mathbf{y}}$. For linearly polarized excitation, contributions arise from those terms with $(l, m) = (1, 0)$, $(2, 0)$, and $(2, \pm 2)$. For the case of circularly polarized excitation, i.e., $(\xi, \eta) = 2^{-1/2}(1, \pm i)$, the only possible contribution arises from the term with $(l, m) = (2, \pm 2)$. This is also readily seen from Eq. (12a), which shows that the electric dipole moment vanishes for circularly polarized excitation since $\hat{\boldsymbol{\epsilon}}_0 \cdot \hat{\boldsymbol{\epsilon}}_0 = 0$.

2. Experimental Observables

The fundamental experimental observable is the radiated SH power per unit solid angle. For detection through an analyzer passing polarization state $\hat{\boldsymbol{\epsilon}}$, this quantity is given by $d\mathcal{P}_{2\omega}/d\Omega = cr^2\varepsilon_1^{1/2}(2\omega)|\hat{\boldsymbol{\epsilon}}^* \cdot \mathbf{E}^{(2\omega)}(\mathbf{r})|^2/(2\pi)$. Writing this quantity in terms of the moments defined above, we have

$$\frac{d\mathcal{P}_{2\omega}(\hat{\boldsymbol{\epsilon}}_0, \hat{\mathbf{k}} \to \hat{\boldsymbol{\epsilon}}, \hat{\mathbf{K}})}{d\Omega} = \frac{cK_1^4}{2\pi[\varepsilon_1(2\omega)]^{3/2}}\left\{|\hat{\boldsymbol{\epsilon}}^* \cdot \mathbf{p}|^2 + \left(\frac{K_1}{6}\right)^2|\hat{\boldsymbol{\epsilon}}^* \cdot \mathbf{Q}(\hat{\mathbf{K}})|^2 - \frac{K_1}{3}\mathrm{Im}[(\hat{\boldsymbol{\epsilon}}^* \cdot \mathbf{p})(\hat{\boldsymbol{\epsilon}} \cdot \mathbf{Q}(\hat{\mathbf{K}})^*)]\right\}. \tag{19a}$$

With respect to the parameters p_0 and κ, we can write alternatively

$$\frac{d\mathcal{P}_{2\omega}(\hat{\boldsymbol{\epsilon}}_0, \hat{\mathbf{k}} \to \hat{\boldsymbol{\epsilon}}, \hat{\mathbf{K}})}{d\Omega} = \frac{cK_1^4|p_0|^2}{2\pi[\varepsilon_1(2\omega)]^{3/2}}|(\hat{\boldsymbol{\epsilon}}_0 \cdot \hat{\boldsymbol{\epsilon}}_0)(\hat{\boldsymbol{\epsilon}}^* \cdot \hat{\mathbf{k}}) - \kappa(\hat{\mathbf{K}} \cdot \hat{\boldsymbol{\epsilon}}_0)(\hat{\boldsymbol{\epsilon}}^* \cdot \hat{\boldsymbol{\epsilon}}_0)|^2. \tag{19b}$$

Without output polarization analysis, we have[24]

$$\frac{d\mathcal{P}_{2\omega}(\hat{\boldsymbol{\epsilon}}_0, \hat{\mathbf{k}} \to \hat{\mathbf{K}})}{d\Omega} = \frac{cK_1^4}{2\pi[\varepsilon_1(2\omega)]^{3/2}}\left\{|\mathbf{p}|^2[1 - (\hat{\mathbf{K}} \cdot \hat{\mathbf{k}})^2] + \left(\frac{K_1}{6}\right)^2|\mathbf{Q}(\hat{\mathbf{K}})|^2[1 - |\hat{\mathbf{K}} \cdot \hat{\boldsymbol{\epsilon}}_0|^2] + \frac{K_1}{3}\mathrm{Im}[(\hat{\mathbf{K}} \cdot \mathbf{p})(\hat{\mathbf{K}} \cdot \mathbf{Q}(\hat{\mathbf{K}})^*)]\right\}, \tag{20a}$$

where we have employed the relation $\mathbf{p} \cdot \mathbf{Q}(\hat{\mathbf{K}})^* = 0$. Equivalently,

$$\frac{d\mathcal{P}_{2\omega}(\hat{\boldsymbol{\epsilon}}_0, \hat{\mathbf{k}} \to \hat{\mathbf{K}})}{d\Omega} = \frac{cK_1^4|p_0|^2}{2\pi[\varepsilon_1(2\omega)]^{3/2}}|(\hat{\boldsymbol{\epsilon}}_0 \cdot \hat{\boldsymbol{\epsilon}}_0) \times [\hat{\mathbf{k}} - \hat{\mathbf{K}}(\hat{\mathbf{K}} \cdot \hat{\mathbf{k}})] - \kappa(\hat{\mathbf{K}} \cdot \hat{\boldsymbol{\epsilon}}_0) \times [\hat{\boldsymbol{\epsilon}}_0 - \hat{\mathbf{K}}(\hat{\mathbf{K}} \cdot \hat{\boldsymbol{\epsilon}}_0)]|^2. \tag{20b}$$

We can simplify Eq. (20b) for cases of linearly and circularly polarized pump radiation to obtain, respectively,

$$\frac{d\mathcal{P}^{lp}_{2\omega}(\hat{\boldsymbol{\epsilon}}_0, \hat{\mathbf{k}} \to \hat{\mathbf{K}})}{d\Omega} = \frac{cK_1^4|p_0|^2}{2\pi[\varepsilon_1(2\omega)]^{3/2}}[1 + |\kappa|^2(\hat{\mathbf{K}} \cdot \hat{\boldsymbol{\epsilon}}_0)^2 - |(\hat{\mathbf{K}} \cdot \hat{\mathbf{k}}) - \kappa(\hat{\mathbf{K}} \cdot \hat{\boldsymbol{\epsilon}}_0)^2|^2], \tag{21a}$$

$$\frac{d\mathcal{P}^{cp}_{2\omega}(\hat{\boldsymbol{\epsilon}}_0, \hat{\mathbf{k}} \to \hat{\mathbf{K}})}{d\Omega} = \frac{cK_1^6|q_0|^2}{2^5 3^2\pi[\varepsilon_1(2\omega)]^{3/2}} \times [1 - (\hat{\mathbf{K}} \cdot \hat{\mathbf{k}})^4]. \tag{21b}$$

Note that the handedness of the circularly polarized radiation does not affect this result, as expected in view of the lack of dependence on possible chiral surface re-

sponse. Integrating Eqs. (21a) and (21b) over all solid angles, we deduce the corresponding total radiated SH power as

$$\mathcal{P}_{2\omega}^{lp} = \frac{2^2 c K_1^4 |p_0|^2}{15[\varepsilon_1(2\omega)]^{3/2}}(5 + |\kappa|^2), \tag{22a}$$

$$\mathcal{P}_{2\omega}^{cp} = \frac{c K_1^6 |q_0|^2}{90[\varepsilon_1(2\omega)]^{3/2}}. \tag{22b}$$

Let us return to the case where we analyze the polarization state of the SH radiation. Two natural choices exist: the analyzer parallel (along $\hat{\boldsymbol{\theta}}$) or perpendicular (along $\hat{\boldsymbol{\varphi}}$) to the scattering plane defined by $\hat{\mathbf{k}}$ and $\hat{\mathbf{K}}$. We denote these arrangements as $\parallel$ and $\perp$, respectively. For fundamental radiation polarized along the x direction, we then obtain the quantities

$$\left.\frac{d\mathcal{P}_{2\omega}}{d\Omega}\right|_{x\to\parallel} = \frac{c K_1^4 |p_0|^2}{2\pi[\varepsilon_1(2\omega)]^{3/2}}\left|\sin\theta + \frac{1}{2}\kappa \sin 2\theta \cos^2\varphi\right|^2, \tag{23a}$$

$$\left.\frac{d\mathcal{P}_{2\omega}}{d\Omega}\right|_{x\to\perp} = \frac{c K_1^6 |q_0|^2}{2^5 3^2 \pi[\varepsilon_1(2\omega)]^{3/2}} \sin^2\theta \sin^2 2\varphi, \tag{23b}$$

for the power per unit solid angle for radiation along these two principal directions.

From symmetry considerations, the case of a fixed input (linear) polarization (along $\hat{\mathbf{x}}$) and a scattering direction specified by (θ, φ) is equivalent to a geometry in which the scattering plane is fixed as $(\theta, \varphi = 0)$ and an input polarization angle of $\psi = -\varphi$ is chosen relative to the x axis. In this alternative geometrical picture, Eqs. (23a)–(23b) become

$$\left.\frac{d\mathcal{P}_{2\omega}}{d\Omega}\right|_{\psi\to\parallel} = \frac{c K_1^4 |p_0|^2}{2\pi[\varepsilon_1(2\omega)]^{3/2}}\left|\sin\theta + \frac{1}{2}\kappa \sin 2\theta \cos^2\psi\right|^2, \tag{24a}$$

$$\left.\frac{d\mathcal{P}_{2\omega}}{d\Omega}\right|_{\psi\to\perp} = \frac{c K_1^6 |q_0|^2}{2^5 3^2 \pi[\varepsilon_1(2\omega)]^{3/2}} \sin^2\theta \sin^2 2\psi. \tag{24b}$$

We define a useful function that describes the (input) polarization anisotropy as

$$\mu(\theta) \equiv \frac{d\mathcal{P}_{2\omega}/d\Omega|_{\parallel\to\parallel}}{d\mathcal{P}_{2\omega}/d\Omega|_{\perp\to\parallel}} = \frac{d\mathcal{P}_{2\omega}/d\Omega|_{\parallel}}{d\mathcal{P}_{2\omega}/d\Omega|_{\perp}}. \tag{25}$$

The second ratio in this equation refers to the radiated power for the specified input polarization. It is equivalent to the first ratio by virtue of Eq. (24b), which shows that for either $\psi = 0$ or $\pi/2$, the output is always $\parallel$-polarized. In terms of the notation used in Eqs. (23a)–(23b), the numerator and denominator of Eq. (25) are given, respectively, by $d\mathcal{P}_{2\omega}/d\Omega|_{\parallel\to\parallel} = d\mathcal{P}_{2\omega}(\varphi = 0)/d\Omega|_{x\to\parallel} = d\mathcal{P}_{2\omega}(\varphi = 0)/d\Omega|_x$ and $d\mathcal{P}_{2\omega}/d\Omega|_{\perp\to\parallel} = d\mathcal{P}_{2\omega}(\varphi = \pi/2)/d\Omega|_{x\to\parallel} = d\mathcal{P}_{2\omega}(\varphi = \pi/2)/d\Omega|_x$. We may, consequently, also interpret the quantity $\mu(\theta)$ as the azimuthal scattering anisotropy. Using Eqs. (16) and (23)–(25), we obtain for SHRS the simple expression

$$\mu(\theta) = |1 + \kappa \cos\theta|^2. \tag{26}$$

Thus measurement of the quantity $\mu(\theta)$ allows us to determine the complex parameter κ, from which we can deduce both the relative strength and phase of the effective nonlinear susceptibilities χ_1 and χ_2 through Eq. (16).

3. Correction for Heterogeneous Media

While there are several important problems for which the dielectric response of the sphere (ε_2) matches or nearly matches that of the ambient medium (ε_1), we clearly need to have a solution for $\varepsilon_1 \neq \varepsilon_2 \neq \varepsilon'$ to address a broader class of experiments. In this subsection, we consider the general problem. Although the analytic approach needed to solve this problem differs significantly from the vector potential treatment given above, the essential characteristics of the SH scattering process are unchanged. As we demonstrate, all of the earlier results are valid once we introduce appropriate local-field correction factors to account for the linear optical response at the fundamental and harmonic frequencies. We are able to do this through an appropriate redefinition of the relation of coefficients χ_1 and χ_2 to the intrinsic nonlinear response of the medium.

Our treatment of the problem for the heterogeneous system may be regarded as the analog of Mie scattering for the second-order nonlinear response. We briefly outline the method here, with the details presented in Appendix A. For the case of the interface nonlinear response, we first solve for the pump field inside, outside, and on the surface of the sphere in terms of an expansion in partial waves, assuming excitation by an incident plane wave. Second, we set up the nonlinear polarization sources in accordance with Eq. (1). Third, we express the SH fields as a linear combination of partial waves. Finally, we apply the appropriate boundary conditions in the presence of surface nonlinear source polarizations[17,107] to evaluate the coefficients in the expansion and, hence, to determine the total SH fields. For the case of the bulk problem, the electric field in the presence of the bulk source (the so-called particular solution of the Maxwell equations) must be taken into account. Evaluation of the SH field is then performed in a similar fashion to that of the surface problem. The technique described here, it should be noted, is applicable for calculating the SH fields from arbitrary-sized spheres, provided only that sufficiently many terms in the partial wave (or multipole) expansion are retained. In the general case, the solution becomes quite involved. However, in the limit of small spheres, where a leading-order treatment is appropriate, the solution remains simple.

We find that all of the relations for SHG from a spherical particle presented above are still valid provided that we redefine the nonlinear responses χ_1 and χ_2 [Eqs. (14a) and (14b)] as

$$\begin{aligned}\chi_1 \equiv\ & \chi^{(2)}_{s,\perp\perp\perp}[L^{E1}_{\perp}(2\omega)L^{E1}_{\perp}(\omega)L^{E2}_{\perp}(\omega)] \\ & + \chi^{(2)}_{s,\perp\parallel\parallel}\left[\frac{3}{2}L^{E1}_{\perp}(2\omega)L^{E1}_{\parallel}(\omega)L^{E2}_{\parallel}(\omega)\right. \\ & \left. + \frac{5}{2}L^{E1}_{\perp}(2\omega)L^{E1}_{\parallel}(\omega)L^{M1}_{\parallel}(\omega)\right] \\ & - \chi^{(2)}_{s,\parallel\perp\parallel}\left[L^{E1}_{\parallel}(2\omega)L^{E1}_{\perp}(\omega)L^{E2}_{\parallel}(\omega)\right. \\ & - \frac{3}{2}L^{E1}_{\parallel}(2\omega)L^{E2}_{\perp}(\omega)L^{E1}_{\parallel}(\omega) \\ & \left. + \frac{5}{2}L^{E1}_{\parallel}(2\omega)L^{E1}_{\perp}(\omega)L^{M1}_{\parallel}(\omega)\right] + \frac{5}{2}L^{E1}_{\parallel}(2\omega)L^{E1}_{\parallel}(\omega) \\ & \times\left[L^{M1}_{\parallel}(\omega)\left(\gamma - \frac{\delta'}{2}\right) + L^{E2}_{\parallel}(\omega)\left(\gamma + \frac{\delta'}{2}\right)\right], \quad (27a)\end{aligned}$$

$$\begin{aligned}\chi_2 \equiv\ & \chi^{(2)}_{s,\perp\perp\perp}L^{E2}_{\perp}(2\omega)L^{E1}_{\perp}(\omega)L^{E1}_{\perp}(\omega) \\ & - \chi^{(2)}_{s,\perp\parallel\parallel}L^{E2}_{\perp}(2\omega)L^{E1}_{\parallel}(\omega)L^{E1}_{\parallel}(\omega) \\ & + 3\chi^{(2)}_{s,\parallel\perp\parallel}L^{E2}_{\parallel}(2\omega)L^{E1}_{\perp}(\omega)L^{E1}_{\parallel}(\omega). \quad (27b)\end{aligned}$$

Here the new quantities are local-field factors given (for $l = 1, 2$) by

$$L^{El}_{\parallel} = \frac{(2l+1)\varepsilon_1}{l\varepsilon_2 + (l+1)\varepsilon_1}, \quad (28a)$$

$$L^{El}_{\perp} = \frac{\varepsilon_2}{\varepsilon'}L^{El}_{\parallel}, \quad (28b)$$

$$L^{Ml}_{\parallel} = \frac{(2l+1)\mu_2}{l\mu_2 + (l+1)\mu_1}. \quad (28c)$$

In these expressions, the notation of E1, E2, and M1 refers respectively, to electric dipole, electric quadrupole, and magnetic dipole effects, while the subscript denotes the field direction relative to the local surface coordinates of the sphere. In Eq. (28c), we have introduced the magnetic local-field factor $L^{Ml}_{\parallel}$. Since $\mu_1 = \mu_2 = 1$ for the optical response, $L^{Ml}_{\parallel} = 1$, but its inclusion is useful for identifying the origin of the different processes leading to SH scattering. The local-field factors can be obtained from the expression for the fundamental electric field inside the sphere [Eq. (A1)]. They represent enhancement of the corresponding induced multipole moments. It should be observed that the factors in Eqs. (27a)–(27b) enter in the expressions for χ_1 and χ_2 for both the *fundamental* and *SH* frequencies. Note also that the bulk term δ' now appears in the expression for χ_1 [Eq. (27a)], in contrast to the case of the homogeneous media [Eq. (14a)]. This reflects, as discussed below, the modified spatial variation of the fundamental field in the presence of the inhomogeneous dielectric media.

3. DISCUSSION

A. Physical Origin and Nature of SH Radiation

1. Origin

The two leading-order contributions to the SH field for a small sphere of radius a are of $O[(ka)^2]$ and $O[(ka)^3]$. These terms yield five distinct excitation-radiation mechanisms for SHRS, represented schematically as E1 + E1 → E1, E1 + E2 → E1, E1 + M1 → E1, E1 + E1 → E2, and E1+E1→M1. In this notation, the first two symbols refer to the nature of the interaction with the fundamental field, and the third symbol describes the SH emission. The E1 + E2 → E1 interaction represents, for example, electric dipole (E1) emission that arises through a channel of combined electric dipole (E1) and electric quadrupole (E2) excitation. If all five contributions are present, the SH field associated with the local E1 + E1 → E1 interaction will be stronger than the other processes by a factor of the order of $(ka)^{-1}$.

For the problem considered in this paper, electric dipole emission (E1) has no local contributions from the E1 + E1 → E1 excitation process because of the centrosymmetry of the problem. The electric dipole radiation can arise only from the nonlocal interactions of E1 + E2 → E1 and E1 + M1 → E1. Physically, the SH electric dipole moment is generated by the *retardation* of the fundamental field as it propagates through the sphere. The electric quadrupole radiation (E2), on the other hand, is not forbidden by centrosymmetry and can be generated under local excitation through the E1 + E1 → E2 process. Magnetic dipole emission (M1), while of the same order as the quadrupole emission, is absent because of the axial symmetry of the problem. The total SH radiation from a sphere in the Rayleigh limit thus arises from a combination of emission by E1 and E2 processes, both of which are of comparable order in (ka), with $\mathcal{P}_{2\omega} \propto (ka)^6$. The classification of the excitation and emission processes described here can be readily made using the local-field factors present for stratified dielectric media, as embodied in Eqs. (27a)–(27b).

The effective susceptibility for E1 emission, χ_1, is a linear combination of the surface susceptibilities, $\chi^{(2)}_{s,ijk}$, and the bulk susceptibilities, γ and δ', according to Eq. (27a). The effective susceptibility for E2 emission, χ_2, is also a linear combination of $\chi^{(2)}_{s,ijk}$, but does not include any bulk response [Eq. (27b)]. As a consequence of a radiation process determined only by these two parameters, we cannot extract all three symmetry-allowed surface $\chi^{(2)}_{s,ijk}$ tensor elements independently of one another (even in the absence of the bulk terms), regardless of what optical measurements we perform. In contrast, the individual elements of $\chi^{(2)}_{s,ijk}$ can be isolated from isotropic planar surfaces by employing various input and output polarization configurations.[17] It is also worth noting that these different emission channels are not mediated by the same set of surface susceptibility elements. For example, $\chi^{(2)}_{s,\perp\perp\perp}$ permits the E1 + E2 → E1 and E1 + E1 → E2 processes, but not E1 + M1 → E1. The excitation mechanisms and the nonlinear material response that contribute to each interaction are summarized in Table 1.

Before we proceed to our discussion of the radiation patterns, we make a brief comment about the bulk non-

Table 1. Excitation-Radiation Interactions and the Corresponding Nonlinear Material Response[a]

Electromagnetic Process	Nonlinear Optical Susceptibilities
E1 + E2 → E1	$\chi^{(2)}_{s,\perp\perp\perp}$, $\chi^{(2)}_{s,\perp\parallel\parallel}$, $\chi^{(2)}_{s,\parallel\perp\parallel}$, γ, δ'
E1 + M1 → E1	$\chi^{(2)}_{s,\perp\parallel\parallel}$, $\chi^{(2)}_{s,\parallel\perp\parallel}$, γ, δ'
E1 + E1 → E2	$\chi^{(2)}_{s,\perp\perp\perp}$, $\chi^{(2)}_{s,\perp\parallel\parallel}$, $\chi^{(2)}_{s,\parallel\perp\parallel}$

[a] Mechanisms of excitation and radiation that are operative for SHRS, together with nonlinear optical susceptibilities that contribute to each process.

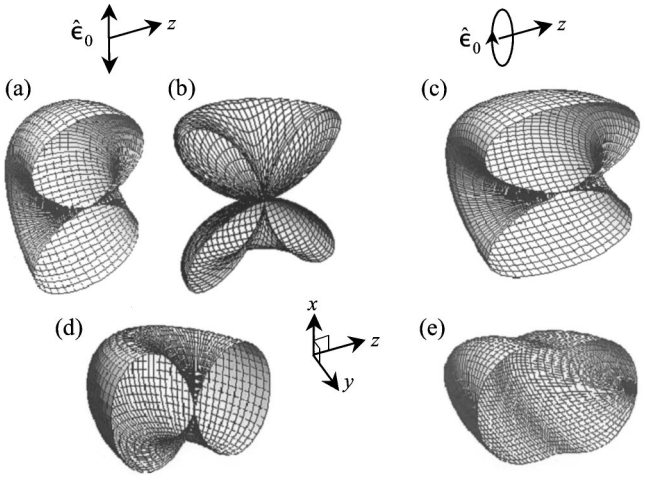

Fig. 2. Graphical representations of scattering patterns $d\mathcal{P}_{2\omega}/d\Omega$ for SHRS [(a)–(c)] and for LRS [(d)–(e)]. Because of symmetry with respect to the x–z plane, only half of each radiation patterns is shown. Panels (a) and (b) are plots of pure E1 (with $\chi_1 \neq 0$ and $\chi_2 = 0$) and E2 (with $\chi_1 = 0$ and $\chi_2 \neq 0$) modes, respectively, for linearly polarized excitation. Panel (c) is a plot of pure E2 mode arising from circularly polarized excitation. For comparison, the LRS radiation patterns are shown for linearly polarized (d) and circularly polarized (e) input radiation.

linear response δ'. This term is absent for the case of homogeneous media [Eq. (14a)], a consequence of the fact that $(\mathbf{E}^{(\omega)} \cdot \nabla)\mathbf{E}^{(\omega)} = 0$ for the assumed plane-wave excitation. However, for *heterogeneous* media, this term does not vanish since the field in the vicinity of the sphere becomes spatially *inhomogeneous*. In particular, the fundamental internal field is no longer purely transverse [Eq. (A1)]. Thus we obtain contributions to the dipole emission from both the γ and δ' terms, as indicated in Eq. (27a), through the E1 + E2 → E1 and E1 + M1 → E1 interactions.

2. Radiation Patterns

The plots of Fig. 2 display the basic SH radiation patterns $d\mathcal{P}_{2\omega}/d\Omega$ for electric dipole and electric quadrupole emission as a function of the scattering direction. Since there is symmetry about the x–z plane, only half of each radiation pattern is depicted. Figures 2(a) and 2(b) correspond to an input field that is polarized along the x direction, while Fig. 2(c) corresponds to circularly polarized input radiation. For comparison, radiation patterns for linear optical scattering (conventional Rayleigh scattering) under linearly and circularly polarized excitation are shown, respectively, in Figs. 2(d) and 2(e). Figure 2(a) illustrates the SH *electric dipole* radiation pattern. We have obtained this result from Eq. (21a) with $\chi_1 \neq 0$ and $\chi_2 = 0$. The plots for the SH *electric quadrupole* radiation patterns are obtained conversely with $\chi_1 = 0$ and $\chi_2 \neq 0$ for linearly polarized and circularly polarized excitation [Figs. (2b) and (2c), respectively]. Note that the E2 radiation patterns differ for linearly and circularly polarized excitation. This behavior arises from the existence of three possible quadrupole modes, corresponding to $(l, m) = (2, 0)$, $(2, 2)$, and $(2, -2)$. All these contributions are present for linearly polarized excitation, while only the $(l, m) = (2, 2)$ or $(2, -2)$ term appears for circularly polarized excitation. In addition, it should be noted that the polarization of the radiated SH field is elliptical in general. This is immediately evident, for example, for the case of circularly polarized incident radiation, which yields a SH field of $\mathbf{E}^{(2\omega)} \propto \hat{\mathbf{K}} \times \mathbf{X}_{2,\pm 2}(\theta, \varphi) \propto \mp i \sin(2\theta)\hat{\boldsymbol{\theta}} + 2\sin(\theta)\hat{\boldsymbol{\varphi}}$.

Let us now consider the general case where both χ_1 and χ_2 are nonvanishing. For a linear polarization state $\hat{\boldsymbol{\epsilon}}_0$, the radiation pattern is fully determined by the parameter κ. We illustrate several distinct cases in Fig. 3. We show both radiation patterns $d\mathcal{P}_{2\omega}/d\Omega$ [(a)–(d)] and the associated values of $\mu(\theta)$ [(e)–(h)]. The four plots of Figs. 3(a)–3(d) correspond to $\kappa = 2$, $-1/2$, -3, and i, respectively. The first three values were chosen to represent a

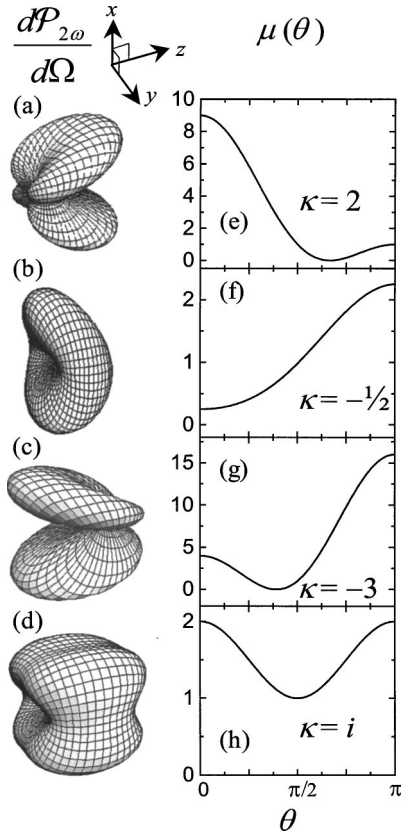

Fig. 3. SH radiation patterns $d\mathcal{P}_{2\omega}/d\Omega$ [(a)–(d)] and polarization anisotropy $\mu(\theta)$ (e)–(h) corresponding to different values of $\kappa \equiv K_1\chi_2/k_1\chi_1 = 2$, $-1/2$, -3, and i. The values $\kappa = 2$, $-1/2$, and -3 correspond to a dominant nonlinear response from $\chi^{(2)}_{s,\perp\perp\perp}$, $\chi^{(2)}_{s,\perp\parallel\parallel}$, or $\chi^{(2)}_{s,\parallel\perp\parallel}$, respectively, for a homogeneous, nondispersive linear optical response. The value $\kappa = i$ illustrates the absence of interference between E1 and E2 modes.

Table 2. Directional and Polarization Selection Rules[a]

Selection Rule	Condition	$\frac{d\mathcal{P}_{2\omega}}{d\Omega}$	Description
Directional	$\hat{\mathbf{k}} \parallel \hat{\mathbf{K}}$	0	Axial SR
Polarization	$\hat{\boldsymbol{\epsilon}}_0 = \hat{\boldsymbol{\epsilon}}_\perp$, $\hat{\boldsymbol{\epsilon}}$ arbitrary	$\propto\lvert(\hat{\boldsymbol{\epsilon}}_0 \cdot \hat{\boldsymbol{\epsilon}}_0)(\hat{\boldsymbol{\epsilon}}^* \cdot \hat{\mathbf{k}})\rvert^2$	Pure E1 emission
	$\hat{\boldsymbol{\epsilon}}_0 = \hat{\boldsymbol{\epsilon}}_\perp$, $\hat{\boldsymbol{\epsilon}} = \hat{\boldsymbol{\epsilon}}_\perp$	0	$\perp \rightarrow \perp$ forbidden
	$\hat{\boldsymbol{\epsilon}}_0$ arbitrary, $\hat{\boldsymbol{\epsilon}} = \hat{\boldsymbol{\epsilon}}_\perp$	$\propto\lvert(\hat{\mathbf{K}}\cdot\hat{\boldsymbol{\epsilon}}_0)(\hat{\boldsymbol{\epsilon}}^* \cdot \hat{\boldsymbol{\epsilon}}_0)\rvert^2$	Pure E2 emission
	$\hat{\boldsymbol{\epsilon}}_0 = \hat{\boldsymbol{\epsilon}}_\parallel$, $\hat{\boldsymbol{\epsilon}} = \hat{\boldsymbol{\epsilon}}_\perp$	0	$\parallel \rightarrow \perp$ forbidden
	$\hat{\boldsymbol{\epsilon}}_0$ circularly polarized	$\propto[1 - (\hat{\mathbf{k}}\cdot\hat{\mathbf{K}})^4]$	Pure E2 emission

[a] Directional and polarization selection rules for SHRS. Here, $\hat{\boldsymbol{\epsilon}}_\perp \propto \hat{\mathbf{K}} \times \hat{\mathbf{k}}$ and $\hat{\boldsymbol{\epsilon}}_\parallel \propto (\hat{\mathbf{K}} \times \hat{\mathbf{k}}) \times \hat{\mathbf{k}}$ are vectors perpendicular and parallel to the scattering plane, respectively.

dominant response from each of the symmetry-allowed surface nonlinear susceptibility elements ($\chi^{(2)}_{s,\perp\perp\perp}$, $\chi^{(2)}_{s,\perp\parallel\parallel}$, and $\chi^{(2)}_{s,\parallel\perp\parallel}$, respectively). In these plots, the ambient is treated as dispersionless, in accordance with the assumptions leading to Eqs. (14a) and (14b). The last case of $\kappa = i$ illustrates the effect of a relative phase difference between χ_1 and χ_2. This situation may arise when the wavelength of the fundamental or SH radiation lies near dipolar or quadrupolar resonances.[24] For the case of $\kappa = i$, the dipole and quadrupole radiation fields are out of phase and do not interfere with one another. Thus the radiation pattern retains its symmetry about $\theta = \pi/2$. For the general case where κ has a real part, as for (a)–(c), the fields from the dipole and quadrupole modes interfere and an asymmetric pattern results, which reflects the sign of Re[κ].

3. Selection Rules

The SHRS process obeys several distinctive selection rules (SR). Table 2 summarizes the key relations. They have been classified, for convenience, as relating either to the directional emission characteristics or to the polarization properties. For the case of directional SR, we observe that SH radiation is strictly zero along the axial direction of $\hat{\mathbf{K}} = \pm\hat{\mathbf{k}}$, i.e., there is neither forward nor backward scattering along the direction of the input wave. The axial SR can be obtained, for example, from the expression for $d\mathcal{P}_{2\omega}/d\Omega$ in Eq. (20b), which clearly vanishes for $\hat{\mathbf{k}} = \hat{\mathbf{K}}$ ($\hat{\mathbf{K}} \perp \hat{\boldsymbol{\epsilon}}_0$). From symmetry considerations, one can in fact show that the axial SR holds true for spheres of arbitrary radius, even outside the Rayleigh limit.

For the case of the polarization properties, several SR can be identified. First, we consider linearly polarized excitation: (a) If the input polarization is perpendicular to the scattering plane, one obtains purely dipolar SH emission [Eq. (19b)]; (b) if the analyzer is set to measure an output polarization that is perpendicular to the scattering plane, one obtains purely quadrupolar SH emission [Eq. (19b)]; and (c) the polarization configurations of $\parallel \rightarrow \perp$ and $\perp \rightarrow \perp$ are forbidden [Eq. (24b)]. For circularly polarized excitation, the SH emission is in a pure ($l = 2, m = \pm 2$) quadrupolar mode [Eqs. (18) and (21b)].

4. Frequency Dependence

An important issue is the spectral response of the SHRS process. In this discussion, we summarize the key results and extend some aspects of our earlier analysis.[24] It is first worth noting that the SHRS process exhibits a strong frequency dependence even in the absence of any dispersion in the linear and nonlinear response of the material. As discussed above, the basic scattering mechanism leads to a frequency dependence of the scattered power $\propto\omega^6$. This dependence will, of course, be modified by the inherent frequency dependence of the nonlinear optical response of the surface (as manifested in $\vec{\vec{\chi}}^{(2)}_s$) and, to the degree present, of the bulk (as manifested in $\vec{\vec{\chi}}^{(2)}_b$). This feature is, of course, of critical importance, since it permits new interface-specific spectroscopic measurements to be carried out on small particles. The general spectroscopic characteristics of such measurements will reflect, as for the analogous measurements on planar interfaces, the presence of resonances at either fundamental or SH frequency. Again in analogy with the case of planar interfaces,[17] the actual experimental measurements of the frequency-dependent response also reflect the dispersion of the linear optical response of the media, as incorporated in the frequency dependence of the dielectric functions ε_1, ε_2, and ε'. Their influence is manifested through what we have designated as the local-field factors of Eqs. (28a)–(28c).

A particularly interesting issue concerns the influence of the linear optical response for materials with Re[ε_2] < 0. For such materials, the spheres may be able to support localized plasmon resonances (LPR). From the local-field factors of Eqs. (28a)–(28c), we see that the resonance occurs when the real part of the denominator of $L^{El}_\parallel$ vanishes, i.e., for

$$\mathrm{Re}[l\varepsilon_2(\Omega)] + (l+1)\varepsilon_1(\Omega) = 0. \tag{29}$$

This condition actually specifies several distinct resonances: Both the $l = 1$ and $l = 2$ modes may be excited, each one either by single- ($\Omega = \omega$) or two-photon excitation ($\Omega = 2\omega$). This leads to *four* distinct resonant frequencies. The presence of enhancement corresponding to resonances at either the fundamental or SH frequency is expected for such a nonlinear optical process. What is remarkable about this situation is that the electric dipole ($l = 1$) LPR and the electric-quadrupole ($l = 2$) LPR appear with comparable importance. Normally, one would expect successive multipole orders to drop sharply with respect to one another in the limit of small-particle size. The present phenomenon is, of course, just a reflection of the analogous effect in the excitation-radiation mecha-

nism for SHRS, where E1 and E2 terms appear on equal footing because of the symmetry property of the problem.

We now analyze explicitly the influence of LPRs in the context of a small metal sphere treated within the Drude model. For the dielectric function of the sphere, we write $\varepsilon_2 = \varepsilon_0 - \omega_p^2/[\omega(\omega + i\gamma_p)]$, where ε_0 is the dielectric function associated with bound charges, ω_p is the plasma frequency, and γ_p is the damping factor. Equation (29) then yields, for $\varepsilon_1 = 1$, dipole LPRs at frequencies of $\{\omega_p/\sqrt{\varepsilon_0 + 2},\ \omega_p/\sqrt{4(\varepsilon_0 + 2)}\}$, and quadrupole LPRs at frequencies of $\{\omega_p\sqrt{2/(2\varepsilon_0 + 3)},\ \omega_p/\sqrt{2(2\varepsilon_0 + 3)}\}$. As a specific example, we consider applying this model to treat aluminum particles of various sizes. We assume that the surface nonlinearity is dominated by $\chi^{(2)}_{s,\perp\perp\perp}$. For the bulk Drude parameters, we use a plasma energy of $\hbar\omega_p \approx 15.55$ eV and a damping of $\hbar\gamma_p \approx 0.49$ eV, as inferred from experimental values of ε_2.[108] The parameter ε_0 is set equal to 1 since interband transitions are of minor importance for aluminum. The spectral dependence of the enhancement in the total radiated power $\mathcal{P}_{2\omega}$ for metal spheres of radii $a = 2.5$, 5, and 10 nm is shown in Fig. 4, taking into account certain corrections described below. The enhancement is calculated with respect to the SHRS from a spherical shell with an equivalent nonlinear response but of fixed 2.5-nm radius. Results are shown for linearly polarized excitation (panel a) and for circularly polarized excitation (panel b). The role of the polarization of the excitation is also discussed below. With respect to the size dependence of the response, the dominant characteristic arises from the scaling $\mathcal{P}_{2\omega} \propto a^6$.

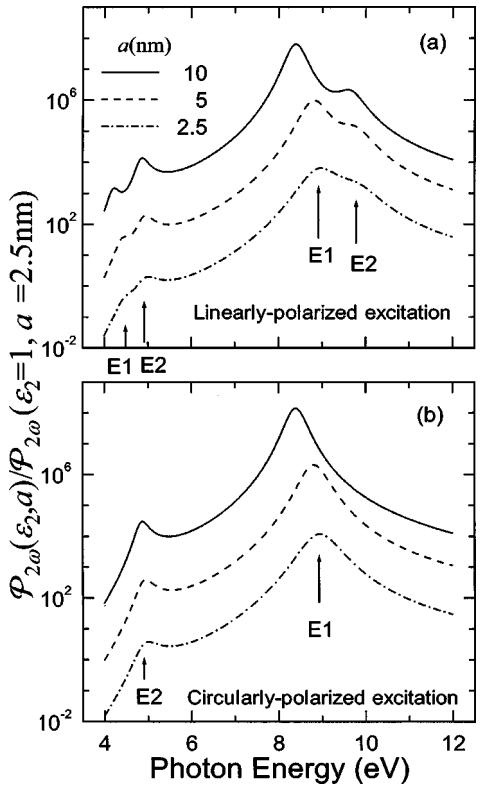

Fig. 4. Spectral dependence of the total SH power, $\mathcal{P}_{2\omega}$, for aluminum spheres of radii $a = 2.5$, 5, and 10 nm relative to that from a spherical shell of fixed 2.5-nm radius. Panel (a) shows the results for linearly polarized excitation, and panel (b) shows the corresponding behavior for circularly polarized radiation. The nonlinear response is assumed to be dominated by $\chi^{(2)}_{s,\perp\perp\perp}$. Note that all four localized plasmon resonances appear in (a), but only two occur in (b).

Corrections to the simple analysis have been introduced to make predictions more accurate as the particle size is varied. One of these modifications accounts for the change in the effective dielectric response of the material as the size of the particle decreases and surface scattering becomes more pronounced.[9] This is described by an enhanced scattering rate γ_p in the Drude model parametrization of the dielectric response through the expression $\gamma_p = \gamma_{\text{bulk}} + Av_F/a$. Here γ_{bulk} denotes the scattering rate for the bulk metal (0.49 eV/$\hbar$ for Al[108]), v_F is the Fermi velocity (2×10^6 m/s for Al at room temperature), and the coefficient A is a model-dependent parameter that is set equal to 1 for this calculation.[9] The consequence of this correction is a slight broadening of the width of the LPR, which becomes more pronounced with decreasing particle size. A modification that becomes more significant in the opposite limit of increasing particle size is a finite-size correction for the LPR condition.[86,24] This correction leads to a shift to lower LPR frequencies with increasing particle radius. While these two corrections modify the detailed form of the results, they do not alter the basic characteristics of the resonant features.

For the SH spectra shown in Fig. 4(a) for Al spheres, single-photon E1 and E2 LPRs appear at energies near 9.0 and 9.8 eV, respectively, while the corresponding two-photon features are present for photon energies near 4.5 and 4.9 eV. For circularly polarized pump radiation, for which only the E1 + E1 $\rightarrow$ E2 interaction is present, only single-photon E1 and two-photon E2 LPRs can be supported. The two-photon E1 and one-photon E2 plasmon resonances, hence, vanish, leaving only the two resonant features shown in Fig. 4(b). The response for linear Rayleigh scattering for the same system (not shown) displays just the single E1 resonance at 9.0 eV. In addition to the possibility for spectroscopic studies of both dipole and quadrupole localized plasmons that is afforded by SHRS, it should be noted that exploitation of these pronounced resonances will significantly enhance the detection sensitivity for suitable particles.

A recent experimental study examined the spectral response of silver spheres of 16-nm radius.[47] Distinct dipole and quadrupole LPRs were observed in a two-photon resonance (2ω). As predicted, the two types of resonance are of comparable strength. By selecting appropriate polarization geometries, either a single or double resonance was observed, in accordance with the predictions of this analysis. In particular, that work made use of the configuration $\hat{\boldsymbol{\epsilon}}_0 \perp \hat{\mathbf{K}}$, which yielded a single dipole resonance according to one of the selection rules described above, and for the configuration $\hat{\boldsymbol{\epsilon}}_0 \parallel \hat{\mathbf{K}}$, which yielded both dipole and quadrupole resonances according to Eq. (29).

5. *Limitations of This Treatment*

Although the present approach can be extended to particles of arbitrary size, we restrict ourselves in this work to the investigation of small particles. In this limit,

where only the leading-order multipole moments need to be considered, we are able to obtain explicit analytic solutions for the general problem of arbitrary linear and nonlinear responses of an isotropic system. The restrictions of this analysis for particles of increasing size are clear: Higher-order multipole moments will begin to become significant. The current treatment becomes invalid and the full nonlinear Mie scattering problem, including many more partial waves, must be solved.

We would like to note, however, that the applicability of the treatment is also restricted in the limit of *very small* particle size. This constraint does not arise because of inaccuracies in the solution of the stated nonlinear optics problem. On the contrary, the solutions given herein become increasingly accurate as the multipole expansion becomes more and more precise. The constraints arise from two other factors. First, as the radius of the sphere decreases, the predicted SH signal drops sharply because of strong cancellation effects. This situation implies that minor departures from the spherical geometry that lead to a breaking of the inversion symmetry will have a disproportionate effect. In this context, it should be noted that only those distortions that break the overall inversion symmetry are of special importance. Distortions of the sphere into a slightly ellipsoidal shape, which retains inversion symmetry, would not have a strong effect, while a distortion toward, say, a pyramidal form, would strongly influence the SHG.

The second correction arises from the increasing inaccuracy of the continuum model in which the optical response is described by spatially homogeneous linear and nonlinear susceptibilities. As the dimension of the sphere approaches the atomic length scale, fluctuations in the local atomic and molecular structure obviously introduce corrections to this picture. In the limit of random fluctuations, these corrections can be viewed as producing *incoherent* scattering by a hyper-Rayleigh process.[109–111] Because of the significant cancellation effects in the homogeneous response, the relative importance of these fluctuations will be increased. While this is an interesting and important topic, it lies outside the scope of the present paper. We should note, however, that several other publications have described the surface response of nanoparticles in terms of the superposition of incoherent molecular emission, i.e., as a hyper-Rayleigh process,[39–46] one in which the *coherent* contribution is entirely neglected.

B. Experimental Considerations

1. Signal Strength

The *strength* of the SHRS process is of considerable importance from the experimental viewpoint: Since the nonlinear response arises from a surface layer in the presence of cancellation effects, one may expect relatively weak SH signals. In view of this situation, we examine the radiation efficiency for SHRS through a comparison with the behavior for the much-studied planar interface. We use this result to infer a typical range of experimentally accessible particle sizes.

Consider a collection of N randomly distributed small particles at high dilution. If the concentration is low enough so that the average interparticle separation is considerably larger than the particle radius, the total scattered SH power is simply an incoherent sum of the emission of the individual particles. For a linearly polarized beam impinging on this system, we can write then, according to Eq. (22a), the total radiated SH power for N particles as

$$\mathcal{P}_{2\omega}^{\text{sphere}} = \frac{2^{12}\pi^3}{15^3 cA^2}\sqrt{\varepsilon_1(2\omega)}(ka)^4 k^2 A_s(5 + |\kappa|^2) \times |\chi_1|^2(\mathcal{P}_\omega)^2. \tag{30}$$

Here, $A_s = 4\pi a^2 N$ represents the aggregate area of the spheres, A the cross-sectional area of the fundamental beam, and $\mathcal{P}_\omega$ the incident fundamental power. Experimentally, one can collect the SH radiation using a large solid angle ($\approx$1 sr), in which case Eq. (30) gives an estimate of the experimental SH signal strength. More refined angular resolution will, of course, cause the signal to decrease correspondingly.

It is useful to compare this result with the total SH power radiated from a planar interface,[17,112]

$$\mathcal{P}_{2\omega}^{\text{plane}} = \frac{2^5\pi^3 k^2 \sec^2\theta_P}{\sqrt{\varepsilon_1(2\omega)}\varepsilon_1(\omega)cA}|\mathbf{e}^{(2\omega)} \cdot \tilde{\boldsymbol{\chi}}_P^{(2)} : \mathbf{e}^{(\omega)}\mathbf{e}^{(\omega)}|(\mathcal{P}_\omega)^2, \tag{31}$$

where $\boldsymbol{\chi}_P^{(2)}$ describes the susceptibility tensor in the planar coordinate system; $\mathbf{e}^{(\omega)}$ and $\mathbf{e}^{(2\omega)}$ represent the polarization vectors of the pump and SH fields, respectively, corrected for the Fresnel factors in the interfacial region; and θ_P is the direction of the outgoing SH signal relative to the surface normal.

For the same incident powers, the ratio of these two signals, $\eta \equiv \mathcal{P}_{2\omega}^{\text{sphere}}/\mathcal{P}_{2\omega}^{\text{plane}}$, is then

$$\eta = \frac{2^7}{15^3}(5 + |\kappa|^2)\varepsilon_1(\omega)\varepsilon_1(2\omega)\cos^2\theta_P(ka)^4\frac{A_s}{A}\left|\frac{\chi_1}{\chi_P}\right|^2, \tag{32}$$

where $\chi_P \equiv \mathbf{e}^{(2\omega)} \cdot \boldsymbol{\chi}_P^{(2)} : \mathbf{e}^{(\omega)}\mathbf{e}^{(\omega)}$. In addition to various geometrical and numerical factors, one sees that the signals scale quadratically in the ratio of the relevant susceptibilities and linearly in the ratio of illuminated surface areas. In addition, there is a factor of $(ka)^4$. This term is significant in the limit of small particles, since it may appreciably diminish the signal. Its origin may be understood as follows: The surface layer of the sphere radiates coherently over its entire area of $4\pi a^2$, while full coherence of radiation occurs for the planar geometry over an area of $\sim\lambda^2 = (2\pi/k)^2$, beyond which the radiation adds coherently only in defined directions. This consideration of coherence accounts for two factors of (ka) in the comparison of radiated powers. The extra factor of $(ka)^2$ in Eq. (32) arises from the need to have nonlocal excitation or radiation in the SHG process for the case of a small sphere. For a hemispherical geometry with lower symmetry, this extra factor is absent,[99] as mentioned below in subsection 3.C.1.

To pursue our discussion further, we assume that $\chi_1 \sim \chi_P$ and neglect factors of the order of unity. We can then write Eq. (32) as

$$\eta \approx (ka)^4 A_s/A. \tag{33}$$

For typical experimental conditions, we expect to probe a collection of particles with an aggregate area of A_s that will easily exceed A. Hence we can assume conservatively that $\eta \approx (ka)^4$. With current experimental techniques, one might reasonably assume that SH signals as small as 10^{-4} from that of a planar surface can be measured, i.e., $\eta \approx 10^{-4}$. This would imply $(ka) \sim 0.1$ and suggest that particle sizes down to $a \sim \lambda/(20\pi)$ should be accessible. For optical wavelengths, this corresponds to particles with radii as small as 5–10 nm. The effect of local fields or resonance enhancement may allow one to observe SHRS in still smaller particles.

An interesting question arises concerning the degree to which we can compensate for the decreased signal from each small sphere by a simple increase in their number. From the point of view of optics alone, we would be constrained only by the onset of multiple scattering in the linear propagation of the fundamental and SH fields. This phenomenon could be considered as restricting measurements to a regime of low turbidity. Using a rough analysis, one then would actually conclude that the signal at the onset of turbidity will be constant, irrespective of the particle radius. This observation follows from the fact that the LRS (leading to turbidity) and the SHRS producing the desired signal both scale as a^6 in terms of the scattered power. Practically speaking, however, reaching this limit of constant turbidity may require a very large number of particles. Moreover, to remain in the limit of high dilution (as required to treat the process as a sum of single-particle scattering events) will necessitate a volume that increases rapidly with decreasing particle radius. For the case of an analysis of a concentrated suspension of spherical particles, the reader is referred to Ref. 95.

2. Determination of χ_1 and χ_2

As we have indicated, the complete nonlinear optical response of a sphere in the Rayleigh limit is defined by the two susceptibility coefficients χ_1 and χ_2, which incorporate both the dipole-allowed surface response and the nonlocal bulk response [Eqs. (27a)–(27b)]. In this subsection, we discuss briefly how these parameters may be deduced from experimental measurements. There is, in fact, no unique way of determining the magnitudes of the two coefficients, χ_1 and χ_2, and their relative phase. A few simple geometrical configurations, based on the selection rules described above may, however, be identified to address this problem in a convenient fashion. Let us first consider the determination of the magnitudes $|\chi_1|$ and $|\chi_2|$. In accordance with the polarization selection rules, one may employ the polarization configuration $\perp \rightarrow \parallel$ to extract the magnitude of the dipole response (χ_1) and employ a circularly polarized pump beam to extract the magnitude of the pure quadrupole response (χ_2).

In addition to establishing values for $|\chi_1|$ and $|\chi_2|$, the relative phase of these two nonlinear responses is often of importance. To examine this parameter, one obviously must use a geometry that provides interference between the two responses. One convenient way to accomplish this is to measure the polarization anisotropy parameter

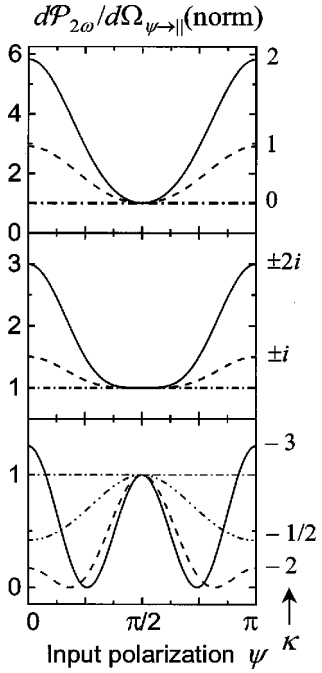

Fig. 5. Normalized SH power $d\mathcal{P}_{2\omega}/d\Omega_{\psi\rightarrow\parallel}$ polarized along the scattering plane at a scattering angle of $\theta = \pi/4$ as a function of the polarization orientation ψ of a linearly polarized pump beam for several values of $\kappa = K_1\chi_2/k_1\chi_1$. The top, middle, and bottom panels indicate cases where κ is real positive ($\kappa = 1, 2$), imaginary ($\kappa = \pm i, \pm 2i$), and real negative ($\kappa = -1/2, -2, -3$), respectively. The case where $\kappa = 0$ is indicated as a horizontal (i.e., no anisotropy) dash-dot line in all panels. A measurement of the quantity $d\mathcal{P}_{2\omega}/d\Omega_{\psi\rightarrow\parallel}$ permits the extraction of the complex polarization anisotropy parameter κ.

$\mu(\theta)$ as discussed in subsection 2.B.2. To obtain $\mu(\theta)$, one takes the ratio of the signal polarized parallel to the scattering plane for incident polarizations parallel and perpendicular to the scattering plane. From this measurement, one can readily determine κ through Eq. (26) and, hence, the complex ratio of χ_2/χ_1. The full determination of χ_1 and χ_2 (up to an overall phase factor) then follows from knowledge of either $|\chi_1|$ or $|\chi_2|$. This method, however, is relatively cumbersome, since it involves adjusting the position of either the detector or the incident laser beam. An experimentally simpler approach to the determination of κ is based on measuring the $\parallel$-polarized SH signal at a single scattering angle θ, while the input polarization angle ψ is varied. As can be seen from Eq. (24a), this procedure also suffices to determine κ. Appropriate scattering angle could be either $\theta = \pi/4$ or $3\pi/4$. These geometries maximize, according to Eq. (23a) or (24a), the quadrupolar contribution, while maintaining interference between the dipole and quadrupole terms. Assuming a fixed scattering angle $\theta = \pi/4$ and normalizing Eq. (24a) with respect to the pure dipole contribution (obtained for $\psi = \pi/2$), we can simplify this expression to $d\mathcal{P}_{2\omega}/d\Omega_{\psi\rightarrow\parallel}(\text{norm.}) = |1 + 2^{-1/2}\kappa\cos^2\psi|^2$. Figure 5 illustrates the dependence of this function on ψ for different values of the parameter κ.

From the experimental standpoint, it should be noted that an absolute determination of the magnitudes $|\chi_1|$ and $|\chi_2|$, as opposed to a relative measurement, will be

quite challenging. In addition to the usual issues of a precise calibration of the parameters of the incident beam and the collection efficiency, one must consider for SHRS the issue of the detected solid angle, the number of nonlinear scatterers, and, ultimately, their radii. Just as for the planar geometry, one might consider the use of a suitably calibrated nonlinear reference. In a simple implementation, this could be a planar nonlinear material with known response that would assist in the calibration of the incident beam and the detection efficiency. Alternatively, one could introduce a reference nonlinear material consisting of small spheres of a material with a known bulk nonlinear response or, more practically, one could make use of molecular hyper-Rayleigh scattering in a suitable liquid.[109,113] Even more challenging would be the experimental determination of the *absolute* phase of χ_1 and χ_2. Such measurements can be carried out readily for the planar geometry by means of interference with a reference signal.[17] Their possible extension to an ensemble of small spheres appears to be difficult, however, since it is unclear how one could introduce a suitable coherent reference signal.

C. Comparison with Other Scattering Processes

1. Comparison with SHG from a Small Hemisphere

In order to understand the distinctive properties of the spherical geometry, it is instructive to compare our findings with a hemispherical geometry. This case, previously investigated in the context of local-field enhancement at roughened metal surfaces,[99] presents an interesting contrast because the hemisphere obviously lacks inversion symmetry.

For our discussion, let us consider a hemisphere with its symmetry axis along z that is embedded in a homogeneous dielectric medium. We assume that only the curved part of the hemisphere generates the SH, and we can calculate the moments [Eqs. (7a)–(7c)] by evaluating the integrals over the appropriate region. Since the overall geometry is clearly not centrosymmetric, the leading-order response is simply the directly excited electric dipole emission, i.e., an E1 + E1 → E1 process. For the SH field, we find $\mathbf{E}_{\mathrm{HS}}^{(2\omega)} \propto (ka)^2 \chi_1^{\mathrm{HS}} \sin\theta \hat{\boldsymbol{\theta}}$ and a total radiated power of $\mathcal{P}^{\mathrm{HS}} \propto (ka)^4 |\chi_1^{\mathrm{HS}}|^2$, where $\chi_1^{\mathrm{HS}} \equiv \chi_{s,\perp\perp\perp}^{(2)} + 3\chi_{s,\perp\parallel\parallel}^{(2)} - 2\chi_{s,\parallel\perp\parallel}^{(2)}$. The effective susceptibility for the stratified media is then modified according to $\chi_{ijk}^{\mathrm{HS}} \rightarrow L_i^{\mathrm{E1}}(2\omega)\chi_{ijk}^{\mathrm{HS}} L_j^{\mathrm{E1}}(\omega) L_k^{\mathrm{E1}}(\omega)$. These results agree with earlier calculations for $\chi_{s,\parallel\perp\parallel}^{(2)}$.[99] As expected here, only the dipolar local-field factors come into play. With respect to the size dependence, we see that the SH field scales as $(ka)^2$, as expected for dipole radiation from the surface of a small object. The need to include a nonlocal interaction for the SH response from the centrosymmetric spherical structure leads to the extra factor of (ka) for the strength of the SH field vis-à-vis the hemispherical geometry, as already discussed above.

2. Comparison with Linear Rayleigh Scattering

It is also informative to compare the results of second-harmonic Rayleigh scattering with the familiar case of linear Rayleigh scattering (LRS). Using the notation that we have introduced in this paper, the radiated electric field for LRS can be written as

$$\mathbf{E}_{\mathrm{sc}}^{(\omega)} = \frac{k^2 \exp(ik_1 r)}{r} (\hat{\mathbf{k}}_{\mathrm{sc}} \times \mathbf{p}_{\mathrm{eff}}^{(\omega)}) \times \hat{\mathbf{k}}_{\mathrm{sc}}, \tag{34}$$

where $\mathbf{p}_{\mathrm{eff}}^{(\omega)} = \mathbf{p}^{(\omega)} = [(\varepsilon_2(\omega) - \varepsilon_1(\omega))/(3\varepsilon_1(\omega))] \times L_{\parallel}^{\mathrm{E1}}(\omega) a^3 E_0 \hat{\boldsymbol{\epsilon}}_0$ is the induced electric dipole moment; $L_{\parallel}^{\mathrm{E1}}(\omega)$ denotes the relevant local-field factor [Eq. (28a)]; and $\hat{\boldsymbol{\epsilon}}_0$ corresponds to the polarization of the incident radiation and $\hat{\mathbf{k}}_{\mathrm{sc}}$ the direction of the scattered light. The principal differences between the LRS and SHRS can be understood by noting that LRS is an electric dipole allowed bulk process, while SHRS derives from a nonlocal surface process. A summary of the overall features of the two scattering processes is presented in Table 3.

The dependence of the radiated power on the frequency and particle size are useful points of comparison. Neglecting the frequency dependence of the material response, we note that the power of LRS scales according to the well-known ω^4 law [Eq. (34)]. This frequency dependence is less sharp than the corresponding ω^6 behavior for SHRS. The difference is attributable to the requirement of nonlocality in the SHRS process. The frequency dependence of the material response enters through local-field factors for both processes. For the nonlinear SHRS, both the incoming and outgoing fields are subject to these effects. As discussed in detail above, quadrupolar local-field factors may appear for SHRS, while for the linear case only the dipolar factor is present. With respect to the dependence of the radiated power on particle radius, however, both scattering processes scale as a^6. For LRS, this corresponds simply to the radiated electric field scaling with particle volume. For SHRS, the same a^6 dependence on particle size is expected. Its origin, however, is somewhat different. It emerges as a consequence of a surface-emission process, with power scaling as the square of the particle *surface area* (a^4), but modified by an additional factor of a^2 imposed by the requirement of nonlocality for SHRS.

Table 3. Comparison of LRS and SHRS[a]

Property	LRS	SHRS
Surface source terms	–	$\chi_{s,\perp\perp\perp}^{(2)}$, $\chi_{s,\perp\parallel\parallel}^{(2)}$, $\chi_{s,\parallel\perp\parallel}^{(2)}$
Bulk source terms	$\varepsilon_2(\omega) - \varepsilon_1(\omega)$	γ, δ'
Emission modes	E1	E1, E2
Mechanism	E1 → E1 (local excitation)	E1 + E2 → E1 E1 + M1 → E1 (nonlocal excitation) E1 + E1 → E2 (local excitation)
Power scaling	$\omega^4 a^6$	$\omega^6 a^6$
Signal along axial direction	Maximal	0
Localized plasmon resonances	1 (E1)	4 (single- and two-photon excitation of E1 and E2)

[a] Comparison of the chief properties of SHRS and LRS for a sphere of radius a at pump frequency ω. E1, M1, and E2 denote, respectively, electric dipole, magnetic dipole, and electric quadrupole contributions.

Under suitable conditions, as indicated above, SHRS originates from an electric dipole moment. It is useful to contrast this radiation process with LRS, which, of course, always occurs by E1 emission. For both processes, the radiation patterns for linearly polarized excitation correspond to emission from an oriented electric dipole. In the case of LRS, the induced moment lies *parallel to polarization vector* $\hat{\boldsymbol{\epsilon}}_0$ of the pump beam. This gives rise to maximal scattering in the forward and backward directions. For the case of SHRS, the dipole exists only because of the presence of the nonlocality. Consequently, it lies parallel to the *direction of propagation* $\hat{\mathbf{k}}$ of the pump beam. The emission pattern is, correspondingly, rotated, with the forward and backward scattering directions now corresponding to minima in the radiation.

The general case of SHRS reflects increased complexity in relation to the LRS process, since both electric dipole and electric quadrupole emission channels are present for the former. In particular, LRS always exhibits mirror symmetry about the plane defined by $\theta = \pi/2$; SHRS does not generally do so (Fig. 3), a consequence of the interference of the two distinct emission modes.

D. Comparison with Previous Theory

A final issue that we would like to discuss concerns comparison of our results with other theories of SHG from spherical particles. Here we restrict our discussion to the aspects of earlier studies that relate to the electrodynamics and nonlinear optics of the problem, as opposed to microscopic models of the response.

Agarwal and Jha were the first to analyze SHG from small spheres.[86] They derived a significant result: the scaling of the SH field with the size parameter ka as $E^{(2\omega)} \sim (ka)^3$. In their analysis, they employed a bulk polarization consisting of the first term of Eq. (3) and a term equal to $\beta \mathbf{E}_{\mathrm{in}}^{(\omega)}(\nabla \cdot \mathbf{E}_{\mathrm{in}}^{(\omega)})$, where β is a coefficient describing the bulk nonlinear response. The δ' term and the surface contributions were not included. Although the β term vanishes in the bulk, it becomes an effective interfacial response (a special case of the surface susceptibilities $\chi_{s,\perp\perp\perp}^{(2)}$ and $\chi_{s,\parallel\perp\parallel}^{(2)}$) for the case of heterogeneous media. In the work of Agarwal and Jha, the γ and β terms yield dipolar and quadrupolar SH radiation through the processes of E1 + M1 $\rightarrow$ E1 and E1 + E1 $\rightarrow$ E2, respectively, consistent with our results. In contrast, however, the full solution presented here for a general surface and bulk nonlinearities also leads to a contribution arising from the quadrupole excitation in the fundamental field [Eq. (A1)], the process that we have denoted as E1 + E2 $\rightarrow$ E1.

More recent electromagnetic calculations examined the surface contribution to SHG in the context of either metal or dielectric particles. In these calculations, only a single surface response, $\chi_{s,\perp\perp\perp}^{(2)}$, was considered. In our analysis, this corresponds to a fixed ratio of χ_2/χ_1 (e.g., of 1 for a homogeneous dielectric). In a noteworthy development, Östling *et al.* and Dewitz *et al.*[96,97] presented a theory of SHG and third-harmonic generation for this case, but for spheres of arbitrary size. They showed that SHG always vanishes along the axial direction. They also demonstrated that for larger spheres, the contribution from higher-order multipoles gives rise to complex angular radiation patterns and can strongly enhance forward scattering. This last behavior is in qualitative agreement with experiments on micron-sized polystyrene spheres,[19,23] where the SH emission is biased toward the forward direction. A comparison between their calculations in the Rayleigh limit [Fig. 4(a) of Ref. 97] and ours [Fig. 3(a) of this work, for the case of $\kappa = 2$] shows some disagreement. The discrepancy seems to arise from the boundary conditions employed. The required boundary conditions for the polarization sheet,[17,107] as used in our analysis [Eqs. (A8a)–(A8d)], should be contrasted with the conventional boundary conditions for the bulk polarization problem.

Martorell *et al.* examined the SHG from dielectric spheres.[78] Assuming the Rayleigh–Gans approximation[3–5] and a dispersionless ambient ($K_1 = 2k_1$), they calculated the SH field from a sphere having a surface nonlinear optical response of $\chi_{s,\perp\perp\perp}^{(2)}$.[106] Although the Rayleigh–Gans approximation is restricted to a class of systems where the indices of refraction of the sphere and ambient media are very close, it has the advantage of facilitating a solution for particles of arbitrary size.[106] Within these restrictions, the calculations of Martorell *et al.* agree with our results. A recent experimental study confirms the validity of that approximation for appropriate material systems.[23] Our model, on the other hand, allows for arbitrary real values of ε_1 and complex values of ε_2 and ε', as is clearly required, for example, for applications to metallic particles. In addition, the effect of dispersion can significantly alter the SH emission properties.

Brudny *et al.*[92] obtained the SH fields for small spheres arising from an inhomogeneous longitudinal pump electric field. Assuming that the field gradient is sufficiently large, they neglected a term arising from retardation effects, corresponding to a contribution of $\nabla[\mathbf{E}^{(\omega)} \cdot \mathbf{E}^{(\omega)}] \propto k\mathbf{E}^{(\omega)} \times \mathbf{B}^{(\omega)}$ to the nonlinear polarization. This condition eliminates the E1 + M1 $\rightarrow$ E1 interaction. As a consequence of consideration of a strongly inhomogeneous pump field, the dipolar SH field scales as (k^2a^3). The quadrupolar SH field predicted by Brudny *et al.*, on the other hand, scales as $(ka)^3$ and occurs through the E1 + E1 $\rightarrow$ E2 process. It is described by an equivalent effective nonlinear susceptibility χ_2 as we have derived.

In a very recent work, Mochán *et al.*[93] performed calculations similar to those in this paper, but for an arbitrary inhomogeneous pump field with spatial variation over a length scale large compared with the particle radius a. The values obtained for the parameters χ_1 and χ_2 are equivalent to those of this work. The agreement between the two calculations is not surprising since the effect of the heterogeneous media as discussed in our paper gives rise to an inhomogeneous field even if the exciting radiation is a plane wave.

4. SUMMARY

We have developed the electromagnetic theory of second-harmonic scattering from the surface and bulk of spheres treated in the Rayleigh limit. In this treatment, we have considered the most general case of symmetry-allowed

surface ($\chi^{(2)}_{s,\perp\perp\perp}$, $\chi^{(2)}_{s,\perp\parallel\parallel}$, and $\chi^{(2)}_{s,\parallel\perp\parallel}$) and bulk ($\gamma$ and δ') susceptibilities for a centrosymmetric and isotropic medium. We find that the surface SH polarization gives rise to two radiation modes, electric dipole and electric quadrupole, that are excited nonlocally and locally, respectively, by the fundamental field. The bulk response, on the other hand, gives rise only to dipolar radiation. These dipole and quadrupole moments are characterized by two effective nonlinear responses, χ_1 and χ_2, that are linear combinations of the surface and bulk susceptibilities and fully define the SH radiation properties of the system. By employing appropriate geometries and polarization combinations, one can extract the amplitudes and relative phase of the two effective nonlinear responses, χ_1 and χ_2.

The SH radiation pattern is characteristic of a combination of the electric dipole and electric quadrupole modes. It obeys a rigorous selection rule against emission in the axial (forward or backward) scattering direction. Other distinctive polarization-selection rules also follow from the nature of the emission process. For the case of a nonresonant SHRS process, the total scattered power $\mathcal{P}_{2\omega}$ scales as $\sim(\omega a)^6$, in contrast to the case of LRS, where $\mathcal{P}_\omega \propto \omega^4 a^6$. In addition, for materials having a dielectric response with $\mathrm{Re}[\varepsilon_2] < 0$, SHRS may exhibit localized plasmon resonance modes associated with the influence of the linear optical response on the nonlinear scattering process. In this case, four localized resonances may arise from the single-photon and two-photon excitation of dipole and quadrupole modes of the sphere. In contrast, in LRS, only a dipole surface resonance is possible. While this interesting prediction has recently been verified experimentally, further measurements are needed to verify fully the applicability of this analysis to practical systems. In particular, the importance of departures from a spherical (or even centrosymmetric) geometry needs further consideration, as does the role of fluctuations associated with the atomic-scale features of small structures.

ACKNOWLEDGMENTS

The authors would like to thank V. Boutou, V. Brudny, K. B. Eisenthal, S. Hill, B. Mendoza, W. L. Mochán, G. Reider, and J. P. Wolf for useful discussions. This work was supported by the Columbia EMSI program under National Science Foundation grant CHE-98-10367 and by the MRSEC program of the National Science Foundation under grant DMR-0213574.

APPENDIX A: SHRS FROM HETEROGENEOUS MEDIA

In this appendix, we calculate the electric field from both surface and bulk polarizations for arbitrary values of the three dielectric functions ε_1, ε_2, and ε'. We assume that ε_1 is real and that all three parameters correspond to material with isotropic linear optical properties.

Let us first consider the pump field at the fundamental frequency ω. From Mie scattering theory,[1] we can write the fundamental electric field inside the sphere ($r < a$) to zeroth and leading orders of (kr) as

$$\mathbf{E}^{(\omega)}_{\mathrm{in}} = L^{E1}_{\parallel}(\omega)\mathbf{E}_0 - \frac{i}{2}L^{M1}_{\parallel}(\omega)\mathbf{r}\times(\mathbf{k}_1\times\mathbf{E}_0) + \frac{i}{2}L^{E2}_{\parallel}(\omega)[(\mathbf{r}\cdot\mathbf{k}_1)\mathbf{E}_0 + (\mathbf{r}\cdot\mathbf{E}_0)\mathbf{k}_1]. \quad \text{(A1)}$$

Here $\mathbf{E}_0$ is the amplitude of the incident field [Eq. (10)], and $L^{\{E,M\}l}_{\parallel}$ are the multipolar field factors given by Eqs. (28a)–(28c). The three terms of Eq. (A1) correspond to an electric dipole (E1), magnetic dipole (M1), and electric quadrupole (E2) excitations of the sphere. (Although $L^{M1}_{\parallel} = 1$ from $\mu_1 = \mu_2 = 1$, this factor is retained in the calculations to identify the nature of the excitation or radiation.)

For analysis of the surface contribution, we must consider the driving field $\mathbf{E}'^{(\omega)}$ at the interface. We write this quantity in terms of radial and tangential components

$$\mathbf{E}'^{(\omega)} = \mathbf{E}'^{(\omega)}_r + \mathbf{E}'^{(\omega)}_t. \quad \text{(A2)}$$

The latter are related to the electric fields just inside the sphere, which are specified above in Eq. (A1) by the relevant boundary conditions of

$$\mathbf{E}'^{(\omega)}_r = \frac{\varepsilon_2(\omega)}{\varepsilon'(\omega)}E^{(\omega)}_{\mathrm{in},r}|_{r=a}, \quad \mathbf{E}'^{(\omega)}_t = \mathbf{E}^{(\omega)}_{\mathrm{in},t}|_{r=a}.$$

This extra factor from the $\varepsilon_2/\varepsilon'$ discontinuity is the origin of the distinction between $L^{\{E,M\}l}_{\parallel}$ and $L^{\{E,M\}l}_{\perp}$ for the local-field factors of the interfacial region given in Eqs. (28a)–(28c).

A. SH Radiation from Surface Contribution

The nonlinear source polarization for the surface is

$$\mathbf{P}^{(2\omega)}_{\mathrm{surface}} = \mathbf{P}^{(2\omega)}_s(\theta,\varphi)\delta(r'-a), \quad \text{(A3)}$$

where

$$\mathbf{P}^{(2\omega)}_s(\theta,\varphi) = \hat{\mathbf{r}}(\chi^{(2)}_{s,\perp\perp\perp}E'_rE'_r + \chi^{(2)}_{s,\perp\parallel\parallel}\mathbf{E}'_t\cdot\mathbf{E}'_t) + 2\chi^{(2)}_{s,\parallel\perp\parallel}E'_r\mathbf{E}'_t, \quad \text{(A4)}$$

and, for simplicity, we have dropped the superscript (ω) on the electric field amplitudes. In this expression, we have several quantities related to the driving fields at the surface. All of these quantities depend only on the angular coordinates (θ, φ). The vector $\mathbf{P}^{(2\omega)}_s(\theta,\varphi)$ may be expressed as an expansion in the basis set of the vector spherical harmonics[114,115] $\{\hat{\mathbf{r}}Y_{lm}(\theta,\varphi), \mathbf{X}_{lm}(\theta,\varphi), \hat{\mathbf{r}}\times\mathbf{X}_{lm}(\theta,\varphi)\}$, which, as described in Appendix B, are related to the spherical harmonics $Y_{lm}(\theta,\varphi)$. Hence, the radial components, $E'_rE'_r$ and $\mathbf{E}'_t\cdot\mathbf{E}'_t$, can be expanded in terms of the spherical harmonics $Y_{lm}(\theta,\varphi)$. The last term of Eq. (A4) possesses no radial component and, hence, may be expanded in terms of the set of basis functions $\{\mathbf{X}_{lm}(\theta,\varphi), \hat{\mathbf{r}}\times\mathbf{X}_{lm}(\theta,\varphi)\}$. Thus we write

$$E'_rE'_r = \sum_{lm} b^{lm}_{\perp\perp\perp}Y_{lm}(\theta,\varphi), \quad \text{(A5a)}$$

$$\mathbf{E}'_t\cdot\mathbf{E}'_t = \sum_{lm} b^{lm}_{\perp\parallel\parallel}Y_{lm}(\theta,\varphi), \quad \text{(A5b)}$$

Table 4. Coefficients b_{ijk}^{lm} for an Incident Field Polarized along x Direction[a]

(l, m)	$b_{\perp\perp\perp}^{lm}/E_0^2$	$b_{\perp\parallel\parallel}^{lm}/E_0^2$	$b_{\parallel\perp\parallel,E}^{lm}/E_0^2$	$b_{\parallel\perp\parallel,M}^{lm}/E_0^2$
(1, 0)	$\frac{4ik_1a}{5}\sqrt{\frac{\pi}{3}}L_{\perp}^{E1}(\omega)L_{\perp}^{E2}(\omega)$	$\frac{2ik_1a}{5}\sqrt{\frac{\pi}{3}}L_{\parallel}^{E1}(\omega) \times [5L_{\parallel}^{M1}(\omega) + 3L_{\parallel}^{E2}(\omega)]$	$\frac{k_1a}{5}\sqrt{\frac{2\pi}{3}}[-5L_{\perp}^{E1}(\omega)L_{\parallel}^{M1}(\omega) + 3L_{\perp}^{E1}(\omega)L_{\parallel}^{E2}(\omega) - 2L_{\perp}^{E2}(\omega)L_{\parallel}^{E1}(\omega)]$	0
(2, 0)	$-\frac{2}{3}\sqrt{\frac{\pi}{5}}[L_{\perp}^{E1}(\omega)]^2$	$\frac{2}{3}\sqrt{\frac{\pi}{5}}[L_{\parallel}^{E1}(\omega)]^2$	$2i\sqrt{\frac{2\pi}{15}}[L_{\perp}^{E1}(\omega)L_{\parallel}^{E1}(\omega)]$	0
(2, ±2)	$\sqrt{\frac{2\pi}{15}}[L_{\perp}^{E1}(\omega)]^2$	$-\sqrt{\frac{2\pi}{15}}[L_{\parallel}^{E1}(\omega)]^2$	$-2i\sqrt{\frac{\pi}{5}}[L_{\perp}^{E1}(\omega)L_{\parallel}^{E1}(\omega)]$	0

[a] Values of the coefficients b_{ijk}^{lm}, defined by Eqs. (A6a)–(A6d), that contribute to the leading-order SH response for an input field with linear polarization along the x direction.

$$2E_r'\mathbf{E}_t' = \sum_{lm}[b_{\parallel\perp\parallel,M}^{lm}\mathbf{X}_{lm}(\theta, \varphi) + b_{\parallel\perp\parallel,E}^{lm}\hat{\mathbf{r}} \times \mathbf{X}_{lm}(\theta, \varphi)]. \tag{A5c}$$

The coefficients $b_{ijk}^{lm} = \{b_{\perp\perp\perp}^{lm}, b_{\perp\parallel\parallel}^{lm}, b_{\parallel\perp\parallel,E}^{lm}, b_{\parallel\perp\parallel,M}^{lm}\}$ are obtained by applying the orthogonality properties of the scalar and vector spherical harmonics:

$$b_{\perp\perp\perp}^{lm} = \int Y_{lm}^* E_r' E_r' \mathrm{d}\Omega, \tag{A6a}$$

$$b_{\perp\parallel\parallel}^{lm} = \int Y_{lm}^* \mathbf{E}_t' \cdot \mathbf{E}_t' \mathrm{d}\Omega, \tag{A6b}$$

$$b_{\parallel\perp\parallel,M}^{lm} = 2\int \mathbf{X}_{lm}^* \cdot E_r'\mathbf{E}_t' \mathrm{d}\Omega, \tag{A6c}$$

$$b_{\parallel\perp\parallel,E}^{lm} = 2\int \hat{\mathbf{r}} \times \mathbf{X}_{lm}^* \cdot E_r'\mathbf{E}_t' \mathrm{d}\Omega. \tag{A6d}$$

Without loss of generality, we can assume that the fundamental radiation is polarized along the $\hat{\mathbf{x}}$ direction. This yields, to leading-order terms, the coefficients b_{ijk}^{lm} for $l = 1$ and 2, given in Table 4.

Neglecting for the moment the bulk nonlinear source polarization, we find that the SH fields inside $(r < a)$ and outside $(r > a)$ the sphere obey the wave equation $\nabla \times \nabla \times \mathbf{E}_{\mathrm{surface},i}^{(2\omega)} - \varepsilon_i(2\omega)K^2\mathbf{E}_{\mathrm{surface},i}^{(2\omega)} = 0$. We may consequently write the fields in terms of the well-known multipole expansion as[104]

$$\mathbf{E}_{\mathrm{surface},i}^{(2\omega)} = \sum_{l=1}^{2}\sum_{m=-l}^{l}\left\{A_M^{(i)}(l, m)f_T^i(K_ir)\mathbf{X}_{lm} + A_E^{(i)}(l, m)\frac{1}{K_i}\nabla \times f_l^i(K_ir)\mathbf{X}_{lm}\right\}, \tag{A7a}$$

$$\mathbf{B}_{\mathrm{surface},i}^{(2\omega)} = \frac{1}{i}\sum_{l=1}^{2}\sum_{m=-l}^{l}\left\{\frac{1}{K}A_M^{(i)}(l, m)\nabla \times f_l^i(K_ir)\mathbf{X}_{lm} + \sqrt{\varepsilon_i(2\omega)}A_E^{(i)}(l, m)f_l^i(K_ir)\mathbf{X}_{lm}\right\}, \tag{A7b}$$

where $f_l^i(K_ir) = \{h_l^{(1)}(K_1r), j_l(K_2r)\}$ are the spherical Hankel functions of the first kind and spherical Bessel functions, corresponding to the scattered field (i = sc or 1) or the internal field (i = in or 2), respectively. In keeping with our interest in the Rayleigh limit, we have retained only the two leading-order ($l = 1, 2$) terms in the expansion. The electric $[A_E^{(i)}(l, m)]$ and magnetic $[A_M^{(i)}(l, m)]$ multipole coefficients, also termed transverse magnetic (TM) and transverse electric (TE) coefficients, respectively, are obtained by applying the boundary conditions below [Eqs. (A8a)–(A8d)] to the fields [Eqs. (A7a)–(A8b)].

Having now decomposed the surface nonlinear source polarization into a suitable set of basis functions, we can find the SH radiation by applying the relevant boundary conditions for a sheet of polarization[17]

$$\Delta D_r^{(2\omega)} = D_r^{(2\omega)}(r = a^+) - D_r^{(2\omega)}(r = a^-) = -4\pi\nabla_t \cdot \mathbf{P}_s^{(2\omega)}, \tag{A8a}$$

$$\Delta\mathbf{E}_t^{(2\omega)} = -\frac{4\pi}{\varepsilon'(2\omega)}\nabla_t P_{s,r}^{(2\omega)}, \tag{A8b}$$

$$\Delta B_r^{(2\omega)} = 0, \tag{A8c}$$

$$\Delta\mathbf{H}_t^{(2\omega)} = 4\pi i\frac{2\omega}{c}\hat{\mathbf{r}} \times \mathbf{P}_s^{(2\omega)}. \tag{A8d}$$

In applying the boundary conditions, we approximate the spherical Hankel and Bessel functions for the limit of small arguments, since we are searching for the leading-order solution for a sphere of small radius. Using $h_l^{(1)}(K_1a) \approx -i(2l - 1)!!/(K_1a)^{l+1}$ and $j_l(K_2a) \approx (K_2a)^l/(2l + 1)!!$, we obtain

$$A_E^{(1)}(l, m) = \frac{4\pi iK_1(K_1a)^{l+1}}{\varepsilon_1(2\omega)(2l + 1)!!}[\chi_{s,\parallel\perp\parallel}^{(2)}b_{\parallel\perp\parallel,E}^{lm}(l + 1)L_{\parallel}^{El}(2\omega) - i(\chi_{s,\perp\perp\perp}^{(2)}b_{\perp\perp\perp}^{lm} + \chi_{s,\perp\parallel\parallel}^{(2)}b_{\perp\parallel\parallel}^{lm})\sqrt{l(l + 1)}L_{\perp}^{El}(2\omega)], \tag{A9a}$$

$$A_M^{(1)}(l, m) = \frac{4\pi iK_1(K_1a)^{l+2}}{\varepsilon_1(2\omega)(2l + 1)!!}\chi_{s,\parallel\perp\parallel}^{(2)}b_{\parallel\perp\parallel,M}^{lm}L_{\parallel}^{Ml}(2\omega). \tag{A9b}$$

Before proceeding to the discussion of the bulk contribution, it should be noted that the technique outlined here to find the response to a surface nonlinearity is general and can be extended to particles of arbitrary size. Naturally, for larger particles, additional partial waves need to be included in the formalism of the driving fields $\mathbf{E}'^{(\omega)}$ at the interface, as well as in the determination of Eqs. (A2)–(A9).

B. SH Radiation from Bulk Contribution

Substituting Eq. (A1) into Eq. (3), we find that the bulk nonlinear source polarization reduces to

$$\mathbf{P}_{\mathrm{bulk}}^{(2\omega)} = ik_1 L_{\parallel}^{E1}(\omega)\left[L_{\parallel}^{M1}(\omega)\left(\gamma - \frac{\delta'}{2}\right) + L_{\parallel}^{E2}(\omega)\left(\gamma + \frac{\delta'}{2}\right)\right]E_0^2\hat{\mathbf{z}}. \tag{A10}$$

To obtain the field inside the sphere, we now solve the *inhomogeneous* wave equation

$$\nabla\times\nabla\times\mathbf{E}_{\mathrm{bulk,in}}^{(2\omega)} - \varepsilon_2(2\omega)K^2\mathbf{E}_{\mathrm{bulk,in}}^{(2\omega)} = 4\pi K^2\mathbf{P}_{\mathrm{bulk}}^{(2\omega)}. \tag{A11}$$

Since $\mathbf{P}_{\mathrm{bulk}}^{(2\omega)} = P_{\mathrm{bulk}}^{(2\omega)}\hat{\mathbf{z}}$ is spatially uniform to leading order, according to Eq. (A10), a particular solution of Eq. (A11) is simply

$$\mathbf{E}_{\mathrm{bulk,in}}^{(2\omega),p} = -\frac{4\pi}{\varepsilon_2(2\omega)}\mathbf{P}_{\mathrm{bulk}}^{(2\omega)}. \tag{A12}$$

Following Eqs. (A7a) and (A7b), we obtain the complementary or general solution to the homogeneous wave equation of Eq. (A11) of

$$\mathbf{E}_{\mathrm{bulk},i}^{(2\omega),c} = \sum_{l=1}^{2}\sum_{m=-l}^{l}\left\{\alpha_M^{(i)}(l,m)f_l^i(K_i r)\mathbf{X}_{lm} + \alpha_E^{(i)}(l,m)\frac{1}{K_i}\nabla\times f_l^i(K_i r)\mathbf{X}_{lm}\right\}, \tag{A13a}$$

$$\mathbf{B}_{\mathrm{bulk},i}^{(2\omega),c} = \frac{1}{i}\sum_{l=1}^{2}\sum_{m=-l}^{l}\left\{\frac{1}{K}\alpha_M^{(i)}(l,m)\nabla\times f_l^i(K_i r)\mathbf{X}_{lm} + \sqrt{\varepsilon_i(2\omega)}\alpha_E^{(i)}(l,m)f_l^i(K_i r)\mathbf{X}_{lm}\right\}. \tag{A13b}$$

To obtain the coefficients $\alpha_{\{M,E\}}^{(i)}$, we apply the conventional boundary matching conditions ($\Delta\mathbf{E}_t^{(2\omega)} = 0$ and $\Delta D_r^{(2\omega)} = 0$) for the net internal field, $\mathbf{E}_{\mathrm{bulk,in}}^{(2\omega)} = \mathbf{E}_{\mathrm{bulk,in}}^{(2\omega),c} + \mathbf{E}_{\mathrm{bulk,in}}^{(2\omega),p}$, and external field, $\mathbf{E}_{\mathrm{bulk,sc}}^{(2\omega)}$. This yields to leading-order the only nonvanishing coefficient

$$\alpha_E^{(1)}(1,0) = \frac{8(K_1 a)^3}{3\varepsilon_1(2\omega)}\sqrt{\frac{2\pi^3}{3}}P_{\mathrm{bulk}}^{(2\omega)}L_{\parallel}^{E1}(2\omega). \tag{A14}$$

The last step in the derivation is to apply a far-field approximation to the vector spherical harmonic expansion to obtain the radiation fields. The large-argument approximation of $h_l^{(1)}(K_1 r) \approx (-i)^{l+1}\exp(iK_1 r)/(K_1 r)$ yields the results quoted above in subsection 2.B.1. Note that in the expressions for the surface [Eq. (A7)] and bulk [Eq. (A13)] SH fields, $A_M^{(1)}(l,m) = 0$ (since $b_{\perp\perp\parallel,M}^{lm} = 0$ from Table 4) and $\alpha_M^{(1)}(l,m) = 0$, respectively, i.e., the emitted fields are of transverse-magnetic character.

APPENDIX B: VECTOR SPHERICAL HARMONICS

The solutions of the vector Laplace and Helmholtz equations in spherical coordinates involve the scalar functions of the radial distance r (spherical Bessel functions) multiplied by three sets of the vector spherical harmonics $\hat{\mathbf{r}}Y_{lm}(\theta,\varphi)$, $\mathbf{X}_{lm}(\theta,\varphi)$, and $\hat{\mathbf{r}}\times\mathbf{X}_{lm}(\theta,\varphi)$. In terms of the spherical harmonic $Y_{lm}(\theta,\varphi)$, the vector spherical harmonic $\mathbf{X}_{lm}(\theta,\varphi)$ is defined as[104]

$$\mathbf{X}_{lm}(\theta,\varphi) = \frac{1}{\sqrt{l(l+1)}}\mathbf{L}Y_{lm}(\theta,\varphi), \tag{B1}$$

where $\mathbf{L} = -i\mathbf{r}\times\nabla$. Explicitly, in spherical coordinates we have

$$\mathbf{X}_{lm}(\theta,\varphi) = \frac{-1}{\sqrt{l(l+1)}}\left\{0, \frac{mY_{lm}(\theta,\varphi)}{\sin\theta}, i\frac{\partial Y_{lm}(\theta,\varphi)}{\partial\theta}\right\}, \tag{B2}$$

and the bracket $\{\}$ denotes the vector components in the $(\hat{\mathbf{r}}, \hat{\boldsymbol{\theta}}, \hat{\boldsymbol{\varphi}})$ basis. The three sets of vector spherical harmonics satisfy a general orthogonality relation

$$\int \mathbf{A}_{lm}^*\cdot\mathbf{B}_{l'm'}\mathrm{d}\Omega = \delta_{\mathbf{AB}}\delta_{ll'}\delta_{mm'}. \tag{B3}$$

Explicit forms of $\mathbf{X}_{lm}(\theta,\varphi)$ for $l = 1, 2$ and $m \geqslant 0$ are listed below:

$$\mathbf{X}_{1,0} = \frac{i}{2}\sqrt{\frac{3}{2\pi}}\{0, 0, \sin\theta\}, \tag{B4a}$$

$$\mathbf{X}_{1,1} = \frac{1}{4}\sqrt{\frac{3}{\pi}}\{0, 1, i\cos\theta\}\exp(i\varphi), \tag{B4b}$$

$$\mathbf{X}_{2,0} = \frac{i}{4}\sqrt{\frac{15}{2\pi}}\{0, 0, \sin 2\theta\}, \tag{B4c}$$

$$\mathbf{X}_{2,1} = \frac{1}{4}\sqrt{\frac{5}{\pi}}\{0, \cos\theta, i\cos 2\theta\}\exp(i\varphi), \tag{B4d}$$

$$\mathbf{X}_{2,2} = \frac{-1}{8}\sqrt{\frac{5}{\pi}}\{0, 2\sin\theta, i\sin 2\theta\}\exp(2i\varphi). \tag{B4e}$$

For negative m values, the corresponding functions can be obtained using the relation

$$\mathbf{X}_{l,-m}(\theta,\varphi) = (-1)^{m+1}\mathbf{X}_{lm}^*(\theta,\varphi). \tag{B5}$$

*E-mail: dadap@phys.columbia.edu.
†E-mail: tony.heinz@columbia.edu.

REFERENCES AND NOTES

1. G. Mie, "Beiträge zur Optik trüber Medien, speziell kolloidaler Metallösungen," Ann. Phys. (Leipzig) **25**, 377–445 (1908).
2. P. Debye, "Der Lichtdruck auf Kugeln von beliebigem Material," Ann. Phys. (Leipzig) **30**, 57–136 (1909).
3. M. Kerker, *The Scattering of Light and Other Electromagnetic Radiation* (Academic, New York, 1969).
4. C. F. Bohren and D. R. Huffman, *Absorption and Scattering of Light by Small Particles* (Wiley, New York, 1983).
5. H. C. van de Hulst, *Light Scattering by Small Particles* (Dover, New York, 1981).
6. N. Bloembergen and P. S. Pershan, "Light waves at the boundary of nonlinear media," Phys. Rev. **128**, 606–622 (1962).
7. C. Flytzanis, F. Hache, M. C. Klein, D. Ricard, and P. Roussignol, "Nonlinear optics in composite materials," Prog. Opt. **29**, 321–411 (1991).
8. U. Kreibig, in *Handbook of Optical Properties*, R. E. Hummel and P. Wißmann, eds. (CRC, Boca Raton, Fla., 1997), Vol. II, p. 145 and references therein.
9. U. Kreibig and M. Vollmer, *Optical Properties of Metal Clusters* (Springer-Verlag, Berlin, 1995).
10. R. F. Haglund, Jr., in *Handbook of Optical Properties*, R. E. Hummel and P. Wißmann, eds. (CRC, Boca Raton, Fla., 1997), Vol. II, p. 191 and references therein.
11. J. L. Cheung, J. M. Hartings, and R. K. Chang, in *Handbook of Optical Properties*, R. E. Hummel and P. Wißmann, eds. (CRC, Boca Raton, Fla., 1997), Vol. II, p. 233, and references therein.
12. S. V. Gaponenko, *Optical Properties of Semiconductor Nanocrystals* (Cambridge University Press, New York, 1998).
13. J. W. Strutt (Lord Rayleigh), "On the light from the sky, its polarization and colour," Philos. Mag. **41**, 107–120, 274–279 (1871).
14. J. F. McGilp, "Optical characterization of semiconductor surfaces and interfaces," Prog. Surf. Sci. **49**, 1–106 (1995).
15. K. B. Eisenthal, "Liquid interfaces probed by second-harmonic and sum-frequency spectroscopy," Chem. Rev. **96**, 1343–1360 (1996).
16. Y. R. Shen, "Wave mixing spectroscopy for surface studies," Solid State Commun. **102**, 221–229 (1997).
17. T. F. Heinz, "Second-order nonlinear optical effects at surfaces and interfaces," in *Nonlinear Surface Electromagnetic Phenomena*, H. Ponath and G. Stegeman, eds. (Elsevier, Amsterdam, 1991) pp. 353–416.
18. J. I. Dadap and T. F. Heinz, "Nonlinear optical spectroscopy of surfaces and interfaces," in *Encyclopedia of Chemical Physics and Physical Chemistry*, J. H. Moore and N. D. Spencer, eds. (Institute of Physics, Bristol, 2001), pp. 1089–1125.
19. H. Wang, E. C. Y. Yan, E. Borguet, and K. B. Eisenthal, "Second harmonic generation from the surface of centrosymmetric particles in bulk solution," Chem. Phys. Lett. **259**, 15–20 (1996).
20. J. M. Hartings, A. Poon, X. Pu, R. K. Chang, and T. M. Leslie, "Second harmonic generation and fluorescence images from surfactants on hanging droplets," Chem. Phys. Lett. **281**, 389–393 (1997).
21. A. Srivastava and K. B. Eisenthal, "Kinetics of molecular transport across a liposome bilayer," Chem. Phys. Lett. **292**, 345–351 (1998).
22. H. Wang, E. C. Y. Yan, Y. Liu, and K. B. Eisenthal, "Energetics and population of molecules at microscopic liquid and solid surfaces," J. Phys. Chem. B **102**, 4446–4450 (1998).
23. N. Yang, W. E. Angerer, and A. G. Yodh, "Angle-resolved second-harmonic light scattering from colloidal particles," Phys. Rev. Lett. **87**, 103902 (2001).
24. J. I. Dadap, J. Shan, K. B. Eisenthal, and T. F. Heinz, "Second-harmonic Rayleigh scattering from a sphere of centrosymmetric material," Phys. Rev. Lett. **83**, 4045–4048 (1999).
25. A. V. Baranov, Ya. S. Bobovich, and V. I. Petrov, "Study of surface-enhanced Raman-scattering initiated by adsorption of molecules on colloidal-silver microparticles," Opt. Spectrosc. **58**, 353–356 (1985) [Opt. Spectrosk. **58**, 578–582 (1985)].
26. C. K. Johnson and S. A. Soper, "Nonlinear surface-enhanced spectroscopy of silver colloids and pyridine: hyper-Raman and second-harmonic scattering," J. Phys. Chem. **93**, 7281–7285 (1989).
27. P. Galletto, P. F. Brevet, H. H. Girault, R. Antoine, and M. Broyer, "Enhancement of the second harmonic response by adsorbates on gold colloids: the effect of aggregation," J. Phys. Chem. B **103**, 8706–8710 (1999).
28. Y. Fang, "Optical absorption of nanoscale colloidal silver: Aggregate band and adsorbate-silver surface band," J. Chem. Phys. **108**, 4315–4318 (1998).
29. H. F. Wang, T. Troxler, A. G. Yeh, and H. L. Dai, "*In situ*, nonlinear optical probe of surfactant adsorption on the surface of microparticles in colloids," Langmuir **16**, 2475–2481 (2000).
30. E. C. Y. Yan, Y. Liu, and K. B. Eisenthal, "*In situ* studies of molecular transfer between microparticles by second-harmonic generation," J. Phys. Chem. B **105**, 8531–8537 (2001).
31. E. C. Y. Yan and K. B. Eisenthal, "Effect of cholesterol on molecular transport of organic cations across liposome bilayers probed by second harmonic generation," Biophys. J. **79**, 898–903 (2000).
32. X.-M. Shang, Y. Liu, E. C. Y. Yan, and K. B. Eisenthal, "Effects of counterions on molecular transport across liposome bilayer: probed by second harmonic generation," J. Phys. Chem. B **105**, 12816–12822 (2001).
33. E. C. Y. Yan, Y. Liu, and K. B. Eisenthal, "New method for determination of surface potential of microscopic particles by second harmonic generation," J. Phys. Chem. B **102**, 6331–6336 (1998).
34. Y. Liu, E. C. Y. Yan, X.-L. Zhao, and K. B. Eisenthal, "Surface potential of charged liposomes determined by second harmonic generation," Langmuir **17**, 2063–2066 (2001).
35. Y. Liu, J. I. Dadap, D. Zimdars, and K. B. Eisenthal, "Study of interfacial charge-transfer complex on TiO_2 particles in aqueous suspension by second-harmonic generation," J. Phys. Chem. B **103**, 2480–2486 (1999).
36. F. W. Vance, B. I. Lemon, and J. T. Hupp, "Enormous hyper-Rayleigh scattering from nanocrystalline gold particle suspensions," J. Phys. Chem. B **102**, 10091–10093 (1998).
37. R. C. Johnson, J. T. Li, J. T. Hupp, and G. C. Schatz, "Hyper-Rayleigh scattering studies of silver, copper, and platinum nanoparticle suspensions," Chem. Phys. Lett. **356**, 534–540 (2002).
38. P. Galletto, P. F. Brevet, H. H. Girault, R. Antoine, and M. Broyer, "Size dependence of the surface plasmon enhanced second harmonic response of gold colloids: towards a new calibration method," Chem. Commun. 581–582 (1999).
39. B. S. Santos, G. A. L. Pereira, D. V. Petrov, C. de Mello Donegá, "First hyperpolarizability of CdS nanoparticles studied by hyper-Rayleigh scattering," Opt. Commun. **178**, 187–192 (2000).
40. D. V. Petrov, B. S. Santos, G. A. L. Pereira, and C. de Mello Donegá, "Size and band-gap dependences of the first hyperpolarizability of $Cd_xZn_{1-x}S$ nanocrystals," J. Phys. Chem. B **106**, 5325–5334 (2002).
41. M. Jacobsohn and U. Banin, "Size dependence of second harmonic generation in CdSe nanocrystal quantum dots," J. Phys. Chem. B **104**, 1–5 (2000).
42. M. J. Eilon, T. Mokari, and U. Banin, "Surface exchange effect on hyper Rayleigh scattering in CdSe nanocrystals," J. Phys. Chem. B **105**, 12726–12731 (2001).
43. C. Landes, M. Braun, and M. A. El-Sayed, "The effect of surface adsorption on the hyper-Rayleigh scattering of large and small CdSe nanoparticles," Chem. Phys. Lett. **363**, 465–470 (2002).
44. M. R. V. Sahyun, "Hyper-Rayleigh scattering (HRS) spectroscopy applied to nanoparticulate TiO_2," Spectrochim. Acta, Part A **58**, 3149–3157 (2002).

45. Y. Zhang, M. Ma, X. Wang, D. Fu, N. Gu, J. Liu, Z. Lu, Y. Ma, L. Xu, and K. Chen, "First-order hyperpolarizability of ZnS nanocrystal quantum dots studied by hyper-Rayleigh scattering," J. Phys. Chem. Solids **63**, 2115–2118 (2002).
46. Y. Zhang, M. Ma, X. Wang, D. G. Fu, H. Q. Zhang, N. Gu, J. Z. Liu, Z. H. Lu, L. Xu, and K. J. Chen, "Second-order optical nonlinearity of surface-capped CdS nanoparticles and effect of surface modification," J. Phys. Chem. Solids **64**, 927–931 (2003).
47. E. C. Hao, G. C. Schatz, R. C. Johnson, and J. T. Hupp, "Hyper-Rayleigh scattering from silver nanoparticles," J. Chem. Phys. **117**, 5963–5966 (2002).
48. S. Roke, W. G. Roeterdink, J. E. G. J. Wijnhoven, A. V. Petukhov, A. W. Kleyn, and M. Bonn, "Vibrational sum frequency scattering from a submicron suspension," Phys. Rev. Lett. **91**, 258302 (2003).
49. J. Nappa, G. Revillod, J.-P. Abid, I. Russier-Antoine, C. Jonin, E. Benichou, H. H. Girault, and P. F. Brevet, "Hyper-Rayleigh scattering of gold nanorods and their relationship with linear assemblies of gold nanospheres," Faraday Discuss. **125**, 145–156 (2004).
50. O. A. Aktsipetrov, P. V. Elyutin, A. A. Nikulin, and E. A. Ostrovskaya, "Size effects in optical second-harmonic generation by metallic nanocrystals and semiconductor quantum dots: the role of quantum chaotic dynamics," Phys. Rev. B **51**, 17591–17599 (1995).
51. O. A. Aktsipetrov, P. V. Elyutin, A. A. Fedyanin, A. A. Nikulin, and A. N. Rubtsov, "Second-harmonic generation in metal and semiconductor low-dimensional structures," Surf. Sci. **325**, 343–355 (1995).
52. T. Kuroda, S. Matsushita, F. Minami, K. Inoue, A. V. Baranov, "Observation of homogeneous broadening in semiconductor nanocrystals by resonant second-harmonic scattering spectroscopy," Phys. Rev. B **55**, R16041–R16044 (1997).
53. R. Antoine, M. Pellarin, B. Palapant, M. Broyer, B. Prével, P. Galletto, P. F. Brevet, and H. H. Girault, "Surface plasmon enhanced second harmonic response from gold clusters embedded in an alumina matrix," J. Appl. Phys. **84**, 4532–4536 (1998).
54. A. Brysch, G. Bour, R. Neuendorf, and U. Kreibig, "Nonlinear optical spectroscopy of embedded semiconductor clusters," Appl. Phys. B **68**, 447–451 (1999).
55. M. L. Sandrock, C. D. Pibel, F. M. Geiger, and C. A. Foss, Jr., "Synthesis and second-harmonic generation studies of noncentrosymmetric gold nanostructures," J. Phys. Chem. B **103**, 2668–2673 (1999).
56. Y. Jiang, P. T. Wilson, M. C. Downer, C. W. White, and S. P. Withrow, "Second-harmonic generation from silicon nanocrystals embedded in SiO_2," Appl. Phys. Lett. **78**, 766–768 (2001).
57. Y. Jiang, L. Sun, and M. C. Downer, "Second-harmonic spectroscopy of two-dimensional Si nanocrystal layers embedded in SiO_2 films," Appl. Phys. Lett. **81**, 3034–3036 (2002).
58. A. M. Malvezzi, M. Allione, M. Patrini, A. Stella, P. Cheyssac, and R. Kofman, "Melting-induced enhancement of the second-harmonic generation from metal nanoparticles," Phys. Rev. Lett. **89**, 087401 (2002).
59. N. Thantu, R. S. Schley, and B. S. Justus, "Tunable room temperature second harmonic generation in glasses doped with CuCl nanocrystalline quantum dots," Opt. Commun. **220**, 203–210 (2003).
60. A. Podlipensky, J. Lange, G. Seifert, H. Graener, and I. Cravetchi, "Second-harmonic generation from ellipsoidal silver nanoparticles embedded in silica glass," Opt. Lett. **28**, 716–718 (2003).
61. R. Bavli, D. Yogev, S. Efrima, and G. Berkovic, "Second harmonic-generation studies of silver metal liquid-like films," J. Phys. Chem. **95**, 7422–7426 (1991).
62. T. Götz, M. Buck, C. Dressler, F. Eisert, and F. Träger, "Optical second-harmonic generation by supported metal-clusters—size and shape effects," Appl. Phys. A **60**, 607–612 (1995).
63. C. P. Collier, R. J. Saykaly, J. J. Shiang, S. E. Heinrichs, and J. R. Heath, "Reversible tuning of silver quantum dot monolayers through the metal-insulator transition," Science **277**, 1978–1981 (1997).
64. T. Muller, P. H. Vaccaro, F. Balzer, and H.-G. Rubahn, "Size dependent optical second harmonic generation from surface bound Na clusters: comparison between experiment and theory," Opt. Commun. **135**, 103–108 (1997).
65. J.-H. Klein-Wiele, P. Simon, and H.-G. Rubahn, "Size-dependent plasmon lifetimes and electron-phonon coupling time constants for surface bound Na clusters," Phys. Rev. Lett. **80**, 45–48 (1998).
66. M. Simon, F. Träger, A. Assion, B. Lang, S. Voll, and G. Gerber, "Femtosecond time-resolved second-harmonic generation at the surface of alkali metal clusters," Chem. Phys. Lett. **296**, 579–584 (1998).
67. B. Lamprecht, A. Leitner, F. R. Aussenegg, "SHG studies of plasmon dephasing in nanoparticles," Appl. Phys. B **68**, 419–423 (1999).
68. S. Baldelli, A. S. Eppler, E. Anderson, Y. R. Shen, and G. A. Somorjai, "Surface enhanced sum frequency generation of carbon monoxide adsorbed on platinum nanoparticle arrays," J. Chem. Phys. **113**, 5432–5438 (2000).
69. T. V. Murzina, A. A. Nikulin, O. A. Aktsipetrov, J. W. Ostrander, A. A. Mamedov, N. A. Kotov, M. A. C. Devillers, and J. Roark, "Nonlinear magneto-optical Kerr effect in hyper-Rayleigh scattering from layer-by-layer assembled films of yttrium iron garnet nanoparticles," Appl. Phys. Lett. **79**, 1309–1311 (2001).
70. O. A. Aktsipetrov, "Nonlinear magneto-optics in magnetic nanoparticles," Colloids Surf., A **202**, 165–173 (2002).
71. R. Srinivasan, Y. Tian, and I. I. Suni, "Surface plasmon effects on surface second harmonic generation during Au nanoparticle deposition onto H-Si(111)," Surf. Sci. **490**, 308–314 (2001).
72. N. Yang, W. E. Angerer, and A. G. Yodh, "Second-harmonic microscopy of single micrometer-size particles on a substrate," Phys. Rev. A **64**, 045801 (2001).
73. H. Unterhalt, G. Rupprechter, and H.-J. Freund, "Vibrational sum frequency spectroscopy on Pd(111) and supported Pd nanoparticles: CO adsorption from ultrahigh vacuum to atmospheric pressure," J. Phys. Chem. B **106**, 356–367 (2002).
74. G. Ma and H. C. Allen, "Diffuse reflection broad bandwidth sum frequency generation from particle surfaces," J. Am. Chem. Soc. **124**, 9374–9375 (2002).
75. H. Tuovinen, M. Kauranen, K. Jefimovs, P. Vahimaa, T. Vallius, J. Turunen, N. V. Tkachenko, and H. Lemmetyinen, "Linear and second-order nonlinear optical properties of arrays of noncentrosymmetric gold nanoparticles," J. Nonlinear Opt. Phys. Mater. **11**, 421–432 (2002).
76. T. S. Koffas, J. Kim, C. C. Lawrence, and G. A. Somorjai, "Detection of immobilized protein on latex microspheres by IR-visible sum frequency generation and scanning force microscopy," Langmuir **19**, 3563–3566 (2003).
77. J. Martorell, R. Vilaseca, and R. Corbalán, "Second harmonic generation in a photonic crystal," Appl. Phys. Lett. **70**, 702–704 (1997).
78. J. Martorell, R. Vilaseca, and R. Corbalán, "Scattering of second-harmonic light from small spherical particles ordered in a crystalline lattice," Phys. Rev. A **55**, 4520–4525 (1997).
79. S. Sato and H. Inaba, "Observation of second harmonic-generation from optically trapped microscopic $LiNbO_3$ particle using Nd-YAG laser," Electron. Lett. **28**, 286–287 (1992).
80. V. Boutou, C. Favre, and J.-P. Wolf, "Femtosecond-laser induced SHG and SFG from charged water microdroplets," in *Conference on Lasers and Electro-Optics*, Vol. 88 of OSA Trends in Optics and Photonics Series (Optical Society of America, Washington, D.C., 2003), paper CMAA4.
81. P. J. Campagnola, M.-D. Wei, A. Lewis, and L. M. Loew, "High-resolution nonlinear optical imaging of live cells by second harmonic generation," Biophys. J. **77**, 3341–3349 (1999).

82. P. J. Campagnola, A. C. Millard, M. Terasaki, P. E. Hoppe, C. J. Malone, and W. A. Mohler, "Three-dimensional high-resolution second-harmonic generation imaging of endogeneous structural proteins in biological tissues," Biophys. J. **81**, 493–508 (2002).
83. L. Moreaux, O. Sandre, S. Charpak, M. Blanchard-Desce, and J. Mertz, "Coherent scattering in multi-harmonic light microscopy," Biophys. J. **80**, 1568–1574 (2001).
84. W. R. Zipfel, R. M. Williams, R. Christie, A. Y. Nikitin, B. T. Hyman, and W. W. Webb, "Live tissue intrinsic emission microscopy using multiphoton-excited native fluorescence and second harmonic generation," Proc. Natl. Acad. Sci. U.S.A. **100**, 7075–7080 (2003).
85. E. C. Y. Yan and K. B. Eisenthal, "Rotational dynamics of anisotropic microscopic particles studied by second harmonic generation," J. Phys. Chem. B **104**, 6686–6689 (2000).
86. G. S. Agarwal and S. S. Jha, "Theory of second harmonic-generation at a metal-surface with surface-plasmon excitation," Solid State Commun. **41**, 499–501 (1982).
87. N. Bloembergen, R. K. Chang, S. S. Jha, and C. H. Lee, "Optical second-harmonic generation in reflection from media with inversion symmetry," Phys. Rev. **174**, 813–822 (1968).
88. X. M. Hua and J. I. Gersten, "Theory of second-harmonic generation by small metal spheres," Phys. Rev. B **33**, 3756–3764 (1986).
89. T. P. Shen and D. Rogovin, "Coherent frequency mixing in microparticle composites," Phys. Rev. A **42**, 4255–4268 (1990).
90. K. Y. Lo and J. T. Lue, "Quantum-size effect on optical second-harmonic generation in small metallic particles," Phys. Rev. B **51**, 2467–2472 (1995).
91. A. Guerrero and B. S. Mendoza, "Model for great enhancement of second-harmonic generation in quantum dots," J. Opt. Soc. Am. B **12**, 559–569 (1995).
92. V. L. Brudny, B. S. Mendoza, and W. L. Mochán, "Second-harmonic generation from spherical particles," Phys. Rev. B **62**, 11152–11162 (2000).
93. W. L. Mochán, J. A. Maytorena, B. S. Mendoza, and V. L. Brudny, "Second harmonic generation in arrays of spherical particles," Phys. Rev. B **68**, 085318 (2003).
94. V. L. Brudny, W. L. Mochán, J. A. Maytorena, and B. S. Mendoza, "Second harmonic generation from a collection of nanoparticles," Phys. Status Solidi B **240**, 518–526 (2003).
95. E. V. Makeev and S. E. Skipetrov, "Second harmonic generation in suspensions of spherical particles," Opt. Commun. **224**, 139–147 (2003).
96. D. Östling, P. Stampfli, and K. H. Bennemann, "Theory of nonlinear-optical properties of small metallic spheres," Z. Phys. D **28**, 169–175 (1993).
97. J. P. Dewitz, W. Hübner, and K. H. Bennemann, "Theory for nonlinear Mie-scattering from spherical metal clusters," Z. Phys. D **37**, 75–84 (1996).
98. K. Hayata and M. Koshiba, "Theory of surface-emitting second-harmonic generation from optically trapped microspheres," Phys. Rev. A **46**, 6104–6107 (1992).
99. C. K. Chen, T. F. Heinz, D. Ricard, and Y. R. Shen, "Surface-enhanced second-harmonic generation and Raman-scattering," Phys. Rev. B **27**, 1965–1979 (1983).
100. G. Berkovic and S. Efrima, "Second harmonic-generation from composite films of spheroidal metal particles," Langmuir **9**, 355–357 (1993).
101. Y. R. Shen, *The Principles of Nonlinear Optics* (Wiley, New York, 1984).
102. For heterogeneous media with $\varepsilon(\text{sphere}) \neq \varepsilon(\text{ambient})$, this term behaves like a polarization sheet at the interface, proportional to the product $\mathbf{E}^{(\omega)}E_r^{(\omega)}$ and, hence, can be incorporated into the surface susceptibilities $\chi^{(2)}_{s,\perp\perp\perp}$ and $\chi^{(2)}_{s,\parallel\perp\parallel}$. The effect of this and any other terms that may contribute in a localized region at the interface is omitted from the analysis. These terms are incorporated in our treatment into the surface nonlinear susceptibility $\vec{\chi}^{(2)}_s$, as has been discussed elsewhere, e.g., see Ref. 17 or P. Guyot-Sionnest and Y. R. Shen, "Bulk contribution in surface second-harmonic generation," Phys. Rev. B **38**, 7985–7989 (1988).
103. L. D. Landau, E. M. Lifshitz, and L. P. Pitaevskii, *Electrodynamics of Continuous Media*, 2nd ed. (Pergamon, New York, 1984), pp. 268–269.
104. J. D. Jackson, *Classical Electrodynamics*, 2nd ed. (Wiley, New York, 1975).
105. The electric dipole, magnetic dipole, and electric quadrupole (tensor) moments are defined as $\mathbf{p} = \int \mathbf{x}\rho(\mathbf{x})\mathrm{d}\mathbf{x}$, $\mathbf{m} = (1/2c)\int \mathbf{x} \times \mathbf{J}(\mathbf{x})\mathrm{d}\mathbf{x}$ and $Q_{ij} = \int[(x_i x_j) - r^2\delta_{ij}] \times \rho(\mathbf{x})\mathrm{d}^3x$, respectively. By employing the relations $\rho(\mathbf{r}) = -\nabla \cdot \mathbf{P}(\mathbf{r})$ and $\mathbf{J}(\mathbf{r}) = -i\Omega\mathbf{P}(\mathbf{r})$, and performing integration by parts, we obtain Eqs. (7a)–(7c).
106. For a sphere of arbitrary radius, an exact expression for the SH electric field for the *homogeneous media* can be obtained without employing the small-particle approximation. This limit (of neglecting differences in the dielectric functions) is known as the SH Rayleigh–Gans approximation, first applied by Martorell *et al.*[78] for the case of a single nonlinear susceptibility element, $\chi^{(2)}_{s,\perp\perp\perp}$, and dispersionless media ($K_1 = 2k_1$). For the case of an isotropic surface having all three nonlinear susceptibility elements $\chi^{(2)}_{s,\perp\perp\perp}$, $\chi^{(2)}_{s,\perp\parallel\parallel}$, and $\chi^{(2)}_{s,\parallel\perp\parallel}$, we substitute Eq. (11) into Eq. (4) with $K_1 = 2k_1$. Making use of Eqs. (5a) and (5b), we obtain $\mathbf{A}(\mathbf{r})$. The resulting SH field in the radiation zone is $\mathbf{E}^{(2\omega)}(\mathbf{r})_{\mathrm{RG}} = [4\pi i \exp(iK_1 r)/r] \times (Ka)^2(E_0^{(\omega)})^2[\Theta(\theta,\varphi)\hat{\boldsymbol{\theta}} + \Phi(\theta,\varphi)\hat{\boldsymbol{\varphi}}]$, where $\Theta(\theta,\varphi)$ and $\Phi(\theta,\varphi)$ are functions given by $\Theta(\theta,\varphi) = \cos(\theta/2)\{[\Gamma_1(\theta) + \Gamma_2(\theta)\cos^2(\theta/2)]f(\varphi) + \Gamma_3(\theta)(\hat{\boldsymbol{\epsilon}}_0 \cdot \hat{\boldsymbol{\epsilon}}_0)\}$ and $\Phi(\theta,\varphi) = -\cos(\theta/2)\Gamma_1(\theta)g(\varphi)$. Here, $f(\varphi) = (\hat{\boldsymbol{\epsilon}}_0 \cdot \hat{\boldsymbol{\rho}})^2$ and $g(\varphi) = (\hat{\boldsymbol{\epsilon}}_0 \cdot \hat{\boldsymbol{\rho}})(\hat{\boldsymbol{\epsilon}}_0 \cdot \hat{\boldsymbol{\varphi}})$, with $\hat{\boldsymbol{\rho}} = \cos\varphi\hat{\mathbf{x}} + \sin\varphi\hat{\mathbf{y}}$ and $\hat{\boldsymbol{\varphi}} = -\sin\varphi\hat{\mathbf{x}} + \cos\varphi\hat{\mathbf{y}}$; $\Gamma_1(\theta) = 2[(\chi^{(2)}_{s,\perp\perp\perp} - \chi^{(2)}_{s,\perp\parallel\parallel})F_1(\theta) - 2\chi^{(2)}_{s,\parallel\perp\parallel}F_2(\theta)]$, $\Gamma_2(\theta) = -(\chi^{(2)}_{s,\perp\perp\perp} - \chi^{(2)}_{s,\perp\parallel\parallel})[F_1(\theta) - 2F_2(\theta)] - 2\chi^{(2)}_{s,\parallel\perp\parallel}[3F_1(\theta) - 2F_2(\theta)]$, and $\Gamma_3(\theta) = -(\chi^{(2)}_{s,\perp\perp\perp} + \gamma)F_1(\theta) - (\chi^{(2)}_{s,\perp\parallel\parallel} + \gamma)[F_1(\theta) - 2F_2(\theta)] + 2\chi^{(2)}_{s,\parallel\perp\parallel}F_1(\theta)$, with the structure factors for $\delta = 2Ka\sin(\theta/2)$ of $F_1(\theta) = (3/\delta^3)[(1 - \delta^2/3)\sin\delta - \delta\cos\delta]$ and $F_2(\theta) = (3/\delta^3)[(1 - \delta^2/2)\sin\delta - \delta(1 - \delta^2/6)\cos\delta]$. (A similar treatment for SFG recently appeared in Ref. 48.) One should note that for the case of *heterogeneous media*, obtaining the SH field requires a full evaluation of Maxwell's equation, as discussed and outlined in the Appendix A of this paper.
107. C. T. Tai, "Equivalent layers of surface-charge, current sheet, and polarization in the eigenfunction-expansions of Green's functions in electromagnetic theory," IEEE Trans. Antennas Propag. **29**, 733–739 (1981).
108. D. Y. Smith, E. Shiles, and M. Inokuti, in *Handbook of Optical Constants of Solids*, E. D. Palik, ed. (Academic, Orlando, 1985), p. 369.
109. R. W. Terhune, P. D. Maker, and C. M. Savage, "Measurements of nonlinear light scattering," Phys. Rev. Lett. **14**, 681–684 (1965).
110. R. Bersohn, Y. H. Pao, and H. L. Frisch, "Double-quantum light scattering by molecules," J. Chem. Phys. **45**, 3184–3198 (1966).
111. P. D. Maker, "Spectral broadening of elastic second-harmonic light scattering in liquids," Phys. Rev. A **1**, 923–951 (1970).
112. V. Mizrahi and J. E. Sipe, "Phenomenological treatment of surface second-harmonic generation," J. Opt. Soc. Am. B **5**, 660–667 (1988).
113. K. Clays and A. Persoons, "Hyper-Rayleigh scattering in solution," Phys. Rev. Lett. **66**, 2980–2983 (1991).
114. E. H. Hill, "The theory of vector spherical harmonics," Am. J. Phys. **22**, 211–214 (1954).
115. P. M. Morse and H. Feshbach, *Methods of Theoretical Physics, Part II*. (McGraw-Hill, New York, 1953), pp. 1898–1901.